CONTRIBUTIONS OF THE INPUT SIGNAL AND PRIOR ACTIVATION HISTORY TO THE DISCHAGE BEHAVIOR OF RAT MOTONEURONES

R.K. Powers, Y. Dai, B.M. Bell*, D.B. Percival* and M.D. Binder

Department of Physiology & Biophysics, School of Medicine, and *Applied Physics Laboratory, University of Washington, Seattle, WA 98195, USA.

Running title: Stimulus and discharge history effects on firing probability

Key words: motoneurones, spike-evoking currents, autoregressive-moving-average (ARMA) model

Section ii. Cell Physiology

Address for correspondence:
Randall K. Powers, Ph.D.
Department of Physiology & Biophysics
University of Washington School of Medicine
Seattle, WA 98195-7290 USA
Tel: 206 221-6325
Fax: 206 685-0619
e-mail: rkpowers@u.washington.edu

SUMMARY

The principal computational operation of neurones is the transformation of synaptic inputs into spike train outputs. The probability of spike occurrence in neurones is determined by the time course and magnitude of the total current reaching the spike initiation zone. The features of this current that are most effective in evoking spikes can be determined by injecting a Gaussian current waveform into a neurone and using spike-triggered reverse correlation to calculate the average current trajectory (ACT) preceding spikes. The time course of this ACT (and the related first-order Wiener kernel) provides a general description of a neurone's response to dynamic stimuli. In many different neurones, the ACT is characterized by a shallow hyperpolarizing trough followed by a more rapid depolarizing peak immediately preceding the spike. The hyperpolarizing phase is thought to reflect an enhancement of excitability by partial removal of sodium inactivation. Alternatively, this feature could simply reflect the fact that interspike intervals that are longer than average can only occur when the current is lower than average toward the end of the interspike interval. Thus, the ACT calculated for the entire spike train displays an attenuated version of the hyperpolarizing trough associated with the long interspike intervals. This alternative explanation for the characteristic shape of the ACT implies that it depends upon the time since the previous spike, i.e., the ACT reflects both previous stimulus history and previous discharge history. The present study presents results based on recordings of noise-driven discharge in rat hypoglossal motoneurones that support this alternative explanation. First, we show that the hyperpolarizing trough is larger in ACTs calculated from spikes preceded by long interspike intervals and minimal or absent in those based on short interspike intervals. Second, we show that the trough is present for ACTs calculated from the discharge of a threshold-crossing neurone model with a post-spike afterhyperpolarization (AHP), but absent from those calculated from the discharge of a model without an AHP. We show that it is possible to represent noise-driven discharge as an autoregressive-moving average (ARMA) process. The ARMA model predicts discharge probability based on the sum of a feedback kernel (AR, autoregressive) and a stimulus kernel (MA, moving average). The feedback

kernel reflects the influence of the AHP, and it increases in amplitude when AHP amplitude is increased by pharmacological manipulations. Finally, we show that the predictions of the ARMA model are virtually identical to those based on the first-order Wiener kernel. This suggests that the Wiener kernels derived from standard white-noise analysis of noise-driven discharge in neurones actually reflect the effects of both stimulus and discharge history.

INTRODUCTION

Neurones compute by transforming the input signals from multiple presynaptic axons into a single train of action potentials transmitted down their own axons. The probability of spike occurrence in the postsynaptic cell depends not only on the amplitude, but also on the time course of the total synaptic current reaching the spike initiation zone. The features of the synaptic current that are most effective in evoking a spike can be estimated by injecting a Gaussian noise current waveform into a cell and using spike-triggered reverse correlation (de Boer & Kuyper, 1968) to determine the average current trajectory preceding spikes (Bryant & Segundo, 1976). Average spike-evoking current trajectories (ACTs) have been calculated in a number of different types of neurones and are generally characterized by a shallow hyperpolarizing trough followed by a more rapid depolarizing peak immediately preceding the spike (Bryant & Segundo, 1976; Mainen & Sejnowski, 1995; Poliakov *et al*. 1997; Binder *et al*. 1999; Svirskis *et al*. 2002, 2004).

The time course of the ACT provides a general description of a neurone's response to dynamic stimuli. A first-order, linear approximation of a neurone's response to a given input can be obtained by convolving the input with the first-order Wiener kernel, which is a scaled, time-reversed version of the ACT (Bryant & Segundo, 1976; Poliakov *et al*. 1997). A number of different specific neurone

properties have been ascribed to ACT time course. For example, the duration of the depolarizing peak in the ACT has been proposed as a measure of the neurone's capacity to detect coincident synaptic inputs, since multiple synaptic inputs arriving within this time window are most likely to generate spikes (cf. Svirskis *et al*. 2004). It has also been suggested that the sharpness of the ACT peak may be related to spike timing precision (Mainen & Sejnowski, 1996; Svirskis & Rinzel, 2003), phase locking (Svirskis *et al*. 2002), and an increased signal-to-noise ratio, which characterizes the neurone's ability to detect small synaptic signals against a background of synaptic noise (Svirskis *et al*. 2002; Svirskis & Rinzel, 2003).

The exact waveform of the ACT is thought to reflect underlying biophysical features of the postsynaptic neurone that may be differentially tuned to promote certain types of behavior. ACT features are thought to depend on both the passive membrane properties of the neurone and on the properties of voltage-activated conductances whose activation and/or inactivation can be modified over voltage ranges subthreshold for spike initiation. Low threshold potassium channels have been shown to contribute to the sharpness of the ACT peak in medial superior olivary neurones (Svirskis *et al*. 2002, 2004). The consensus explanation for the hyperpolarizing trough in the ACT is that the removal of sodium inactivation by hyperpolarizing inputs makes it easier for subsequent depolarizing inputs to evoke spikes (Mainen & Sejnowski, 1995; Poliakov et al. 1997; Binder *et al*. 1999; Fellous *et al*. 2003; Gutkin *et al*. 2003; Svirskis *et al*. 2004). This explanation is consistent with the observation that the hyperpolarizing trough increases in amplitude with increasing depolarizing D.C. bias in the injected current (Bryant & Segundo, 1976). Alternatively, this feature could simply reflect the fact that longer than average interspike intervals can only occur when the current is lower than average toward the end of the interspike interval, and the ACT calculated over the entire spike train reflects this influence. This alternative explanation implies that the shape of the ACT depends upon the time since the previous spike (see also Aguera y Arcas *et al*. 2003), that is, it reflects both previous stimulus history and previous discharge history.

The goals of the present experiments were to determine how the shape of the ACT in a neurone depends on the time since the previous spike, and to obtain separate estimates of the effects of stimulus and discharge history on spiking probability. To do so, we elicited repetitive discharge in rat hypoglossal motoneurones *in vitro* by injecting long currents steps with superimposed noise. We used spike-triggered reverse correlation to compute ACTs from all spikes or only those associated with certain ranges of preceding interspike intervals. We found that the hyperpolarizing phase of the ACT was exaggerated when computed from spikes preceded by long interspike intervals, but minimal or absent for those triggered by spikes preceded by short intervals. These results could be replicated using a simple-threshold crossing neurone model with an AHP. These finding suggests that the hyperpolarizing dip in the ACT does not necessarily reflect the removal of sodium inactivation as previously thought (Mainen & Sejnowski, 1995; Poliakov *et al.* 1997; Binder *et al*. 1999; Fellous *et al*. 2003; Gutkin *et al*. 2003; Svirskis *et al*. 2004), but instead reflects the effects of previous discharge history due to the AHP.

To separate the effects of discharge history and the stimulus on spike probability, we modeled the spike train as an autoregressive-moving average (ARMA) process (Box *et al.* 1994), in which the effects of discharge history are represented by an autoregressive (AR) kernel and the effects of stimulus history by a moving average (MA) kernel. The AR kernels predicted a prolonged (~ 100 ms) decrease in firing rate following a spike. The MA kernels predicted a much briefer (~ 5 ms) increase in rate following a pulse of stimulus current, without the subsequent decrease in firing rate predicted by the standard first-order Wiener kernel. Pharmacological enhancement of the afterhyperpolarization (AHP) current led to a pronounced increase in the amplitude of the AR kernel but relatively minor effects on the MA component. We have also been able to demonstrate that the linear prediction of current-evoked changes in firing probability based on the first-order Wiener kernel represents the sum of the predicted changes based on the AR and MA kernels.

METHODS

Experimental recordings

We made intracellular recordings of spike discharge in rat hypoglossal motoneurones from brainstem slices. Experiments were carried out in accordance with the animal welfare guidelines in place at the University of Washington. Sprague-Dawley rats (16-21 days old) were anesthetized by an intramuscular injection of 1.8 ml/kg of a 5:1.6:6.6 solution of ketamine: xylazine: saline. A section of the brainstem from the mid-medulla to the rostral pons was removed, and we made several 400 μm thick transverse slices containing the hypoglossal (HG) nucleus, as previously described **(**Sawczuk *et al*. 1995; Poliakov *et al*. 1996, 1997). Individual slices were transferred from a holding chamber to the recording chamber, where they were submerged in artificial cerebrospinal fluid (ACSF) at room temperature flowing at a rate of 2 ml/min (e.g., Sawczuk *et al*. 1995). The ACSF contained (in mM): 126 NaCl, 2 KCl, 1.25 NaH_2PO_4, 26 $NaHCO_3$, 2 $MgCl_2$, 2 $CaCl_2$ and 10 glucose. The HG nucleus was identified visually by anatomic position in the slice, and intracellular recordings were obtained using glass electrodes filled with 3 M KCl or K-acetate, with resistances of 20-50 MΩ. Identification of motoneurones was based on location and on the similarity of intrinsic properties to those previously reported (Viana *et al*. 1990; Sawczuk *et al*. 1995, 1997).

After impaling a neurone within the HG nucleus, we measured a number of intrinsic properties, including rheobase (the minimum amplitude of a 50 ms injected current pulse needed to elicit a spike), input resistance, the amplitude of the afterhyperpolarization (AHP) following single spikes elicited at several different mean membrane potentials, and the frequency-current (f-I) relation obtained in response to a series of 1 s injected current pulses of different amplitude. Only those cells capable of sustained repetitive discharge were studied further. We obtained a series of responses to a noisy injected current waveform (described below) superimposed on long current steps of different amplitudes. The command for the injected current waveform was computed and stored as a wave in Igor (Wavemetrics,

Oswego, OR) and output via an Instrutech D/A converter at a sampling rate of 10 KHz. This output waveform was sent to the external current command of an Axoclamp 2B amplifier, operating in either bridge or discontinuous current clamp mode, and the resultant voltage response was also sampled at a rate of 10 KHz and stored as an Igor wave. We measured the number of spikes evoked by the noisy current waveform and changed the amplitude of the current step as necessary in order to obtain several (4 – 9) epochs of discharge at the same mean rate (± 10 %). We then attempted to repeat the entire protocol after switching to a perfusion solution containing 1mM tetraethylammonium (TEA), and again after switching back to control ACSF. The addition of TEA at this concentration produces a partial block of the delayed rectifier potassium current, leading to an increase in spike width and increased calcium influx during the spike, which in turn produces an increase in the amplitude of the medium-duration AHP mediated by the SK-type calcium-activated potassium conductance (see Results, and Viana *et al*. 1993).

Stimulus waveform

The standard injected current waveform was 42 s in duration, and consisted of the following components: (1) a 38 s step starting 2s after the waveform onset, (2) a 26.2 s zero-mean random noise waveform starting 8 s after step onset, (3) the sum of two, 26.2 s trains of transients starting at the same time as the noise waveform, and (4) two series of eight 1 ms, 1 nA hyperpolarizing current pulses applied before and after the current step. The random noise component was filtered, Gaussian noise calculated with the following recursive formula:

$$x(i) = (1 - \Delta t / \tau_f) * x(i-1) + \text{gnoise}(\sigma) * \sqrt{1 - (1 - \Delta t / \tau_f)^2} \text{ for } \tau_f > \Delta t,$$

where x(i) is the i^{th} point of the random waveform, Δt is the sampling interval in ms, gnoise(σ) is a random number drawn from a Gaussian distribution with a mean of zero and a standard deviation of σ,

and τ_f is the filtering time constant. For all trials, the noise standard deviation was set to 0.25 nA and the filtering time constant was 1 ms, but we varied the exact values of the noise from trial to trial by choosing different random number seeds. The trains of transients were two symmetric (positive and negative) alpha functions applied at a mean rate of 40 Hz, with Poisson distributions of intervals. The time-to-peak of the alpha functions was 0.5 ms and the peak amplitudes were ± 0.3 nA. The sum of the train of transients and the random noise component also exhibited a Gaussian amplitude distribution, but with a standard deviation of 0.262 nA.

Computer simulations

We attempted to reproduce the salient features of our experimental data using two different threshold-crossing neurone models. In the basic model, threshold-crossings are followed by an exponentially decaying potassium conductance that produces an AHP. In the alternative model, there is no potassium conductance, but threshold-crossing produces a reset of the voltage for a specified duration. The basic model is similar to that described by Pinsky & Rinzel (1994) in which one compartment represents the soma and proximal dendrites, and the other compartment represents the remainder of the dendritic tree (see also Mainen & Sejnowski 1996; Booth *et al.* 1997). The differential equations governing the behavior of the model are as follows:

$$\frac{dV_s}{dt} = \frac{1}{C_s} * [-G_{ls} * V_s - G_k * (V_s - V_k) + G_c * (V_d - V_s) + I]$$

$$\frac{dV_d}{dt} = \frac{1}{C_d} * [-G_{ld} * V_d + G_c * (V_s - V_d)]$$

$$\frac{dG_k}{dt} = G_k * \exp[-(t - t') / \tau_{Gk}] + G_{kadd} * \delta(t - t'),$$

where V_s, G_{ls} and C_s are the voltage, conductance and capacitance of the somatic compartment, V_d, G_{ld} and C_d are the voltage, conductance and capacitance of the dendritic compartment, G_c is the coupling

conductance between the two compartments, and I is the current injected into the somatic compartment. Spikes occur whenever V_s crosses a specified voltage threshold (V_{th}) and are followed by an increment (G_{kadd}) in a slow K^+ conductance (G_k, with an equilibrium potential V_k) that decays with a time constant t_{Gk}. The model parameters were chosen so that the behavior of the model (i.e., rheobase, input resistance, frequency-current relation and AHP characteristics) fell within the range of behavior observed in rat hypoglossal motoneurones (see RESULTS). Although these behaviors could have been reproduced in a single compartment model, the second compartment was needed in order to reproduce the passive impulse response of motoneurones (i.e., the voltage decay following a subthreshold pulse of current), which is better fit by the sum of two exponentials, rather than the single exponential decay exhibited by a one-compartment model.

Data analysis

The times of spike occurrence were concatenated over several trials with similar mean firing rates and used to calculate: the mean and standard deviation of the interspike intervals (ISIs), the ISI histogram, and the hazard function. The ISI histogram represents an estimate of the underlying probability density function, pdf(t). The hazard function, which represents the instantaneous probability of a spike occurring in an infinitesimal time interval as function of time since the previous spike, is defined as:

$$haz(t) = pdf(t) / (1 - \int_0^t pdf(t)dt).$$

We corrected for finite bin widths in the ISI histogram by approximating the hazard function as the probability of a spike occurring in the next millisecond: $(\ln(N_0/N_1)/bw$, where N_1 is the sum of all the spikes occurring at intervals longer than a particular histogram bin, and N_0 is that number plus the number of spikes occurring in that bin and bw is bin width in ms (cf. Matthews, 1996; Powers & Binder 1996). This probability function can also be expressed as an instantaneous firing rate by multiplying by

1000 (e.g., a process with a probability of a spike occurrence of 0.01 would have a mean firing rate of 10 spikes/s).

The estimated hazard function is subject to sampling variability that will increase with decreasing sample size (i.e., bin counts). Although confidence limits can be calculated for this function (cf. Wetmore & Baker 2004), this procedure is rather complicated and involves calculation of a probability distribution for each individual point in the hazard rate curve based on the assumption that the hazard rate at a particular time is a constant probability binomial process. Since we are using the hazard rate for illustrative purposes only, we have not included errors bars on our hazard rate plots.

Average spike-evoking current trajectories (ACTs) were calculated by averaging the noisy injected current from 100 ms preceding spikes to 20 ms following spikes. We also calculated ACTs for a defined subset of spikes based on the length of the preceding ISI. We assessed the statistical significance of ACT features by calculating 98% confidence limits for the average and standard deviation of the current preceding spikes as described by Bryant and Segundo (1976). For the average, the confidence limits are $\pm$ 2.326 * $\tilde{\sigma}_{ns}$sqrt(N), where σ_{ns} is the standard deviation of the noise waveform and N is the number of spikes. The calculation of the confidence limits for the standard deviation about the mean was based on the following formula:

$$\sigma_{ns} * \{1 - [2 / (9 * N)]\} \pm 2.326 * \sqrt{[2 / (9 * N)]^{3/2}} .$$

We also used the spike times together with the injected noise to estimate the parameters of an autoregressive moving average (ARMA; Box *et al.* 1994) model of spike generation by defining the spike output Y_n and the noisy input X_n as follows: Y_n is a time series that is unity (zero) if there was (was not) a spike) in the nth time interval (nΔt, (n+1) Δt), where n is a nonnegative integer, and Δt is the interval between observations. X_n is a time series that represents the input to the neurone during the nth time interval. The ARMA model consisted of a stimulus kernel (MA, moving average) and a feedback kernel (AR, autoregressive):

$$Y_n = \mu + \sum_{\tau=0}^{q} a_\tau X_{n-\tau} + \sum_{\iota=1}^{p} b_\tau (Y_{n-\tau} - \mu),$$

where μ is the expected value of Y_n; q and p are known positive integers that determine the length of the kernels; and a_τ , b_τ are unknown parameters representing the estimated values of the stimulus kernel and feedback kernel at each time lag τ. In order to reduce the number of parameters to be estimated, we re-sampled the spike times and stimulus waveforms using time intervals of 0.4 ms rather than 0.1 ms. We used a least squares approach to estimate a_τ and b_τ by reformulating the above equation in terms of symmetric Toeplitz matrices (see APPENDIX). The ARMA model relates the spike train and noisy stimulus. It does not predict the zero/one spike train process; rather, any 'predictions' made from the model should be interpreted as probabilities or rates of firing. Higher model output values indicate an interval where a spike is more likely to occur. This technique could be used to predict the spike probability based on only the stimulus kernel, only on the feedback kernel alone or based on a combination of the two kernels. When the analysis is based on the effects of stimulus history alone, the resultant kernel is referred to as the first-order Wiener kernel. We compared the performance of these different models by first calculating peri-stimulus time histograms (PSTHs) describing the effect of the alpha function current transients on firing probability. We then compared the calculated PSTHs to those predicted by convolving the stimulus kernel (or the first-order Wiener kernel) with the current transient and the feedback kernel with the spike times.

Assessment of the statistical significance of differences in the features of ACTs and kernels for different experimental conditions was based on Student's paired t-test.

RESULTS

Intrinsic properties of rat hypoglossal motoneurones

We obtained extensive recordings (> 1000 spikes) of noise-driven discharge from nine rat hypoglossal (HG) motoneurones. In some of the cells, we obtained discharge records at more than one mean rate, resulting in a total database of 14 sets of noise-driven discharge records under control conditions. The nine motoneurones exhibited the following intrinsic properties (mean ± SD, range): rheobase: 0.5 ± 0.2 nA, 0.2 – 0.9; input resistance: 29.8 ± 9.1 MΩ, 21.3 – 46.1; membrane time constant: 6.4 ± 1.9 ms, 4.2 – 9.2; first equalizing time constant: 0.7 ± 0.3 ms, 0.2 – 1.2; afterhyperpolarization (AHP) duration at half amplitude: 56 ± 15 ms, 29 – 79; slope of steady-state frequency current relation: 17.4 ± 5.8 imp/s/nA; 9.3 – 24.1. All of these values are similar to those previously reported for rat HG motoneurones (Viana *et al.* 1994, 1995; Sawczuk *et al.* 1995), except for AHP duration at half amplitude, which is longer than previously reported (Viana *et al.* 1994, 1995).

Features of the average spike-evoking current trajectories (ACTs) in rat HG motoneurones

We computed average spike-evoking current trajectories (ACTs) by averaging the noisy injected current over an interval of from +20 ms to –100 ms with respect to the time of occurrence of each spike in several trials with similar mean firing rates. Figure 1A shows the entire time course of an ACT (lower, thick black trace), as well as the standard deviation about the mean (upper, gray trace), computed for one motoneurone firing at a mean rate of 17.1 imp/s. (The same traces are shown in Figure 1B on an expanded time scale.) The horizontal dashed lines show the 98% confidence limits for the mean (lower lines) and standard deviation (upper lines, see METHODS and Bryant & Segundo, 1976). As previously reported (Bryant & Segundo, 1976; Mainen & Sejnowski 1995; Poliakov *et al.* 1997; Binder *et al*. 1999; Svirskis *et al.* 2002, 2004), the ACT exhibits a shallow trough (lower arrows in Fig. 1A) followed by a sharp peak immediately preceding the spike (time zero). The standard deviation about the average is

reduced significantly starting about 15 ms before the spike (upper arrow in Fig. 1A) and reaches a minimum around the time of the ACT peak. This decrease in variability indicates that action potentials tend to be preceded by current waveforms that are similar to the average trajectory (cf. Bryant & Segundo, 1976). The ACTs showed similar features in all cases, i.e. a relatively long duration trough (23.5 ± 5.9 ms, range: 10.5 – 30.7 ms, n=14), followed by a sharp peak (peak amplitude: 0.37 ± .03 nA, range: .34 - .41 nA). Similarly, the standard deviation about the mean dropped to a minimum around the time of the ACT peak (to 76.0 ± 1.5 % of the control SD) in all cells.

The trough in the ACT might indicate that spikes are more likely to be evoked by depolarization when a preceding hyperpolarization removes some sodium inactivation (see INTRODUCTION). Alternatively, this feature could simply reflect the fact that longer interspike intervals can only occur when the current is lower than average toward the end of the interspike interval (These alternatives are not mutually exclusive; see DISCUSSION.) The latter interpretation is supported by the fact that the ACT trajectory is different for ACTs compiled separately for spikes preceded by intervals shorter than and longer than the median interval. Figure 2 shows ACTs calculated from the same discharge records as those used for figure 1 based on the average current preceding all spikes (thick black traces), only those spikes preceded by interspike intervals shorter than the median ("Short", gray traces) and only those spikes preceded by intervals longer than the median ("Long", thin black traces). The ACT associated with the shorter interspike intervals has the largest peak amplitude and virtually no preceding trough, whereas the ACT associated with the longer interspike intervals has a smaller peak amplitude and a pronounced trough. These features are typical of the differences between ACTs calculated from short and long interspike intervals. Compared to ACTs calculated from longer intervals, ACTs based on shorter intervals had significantly larger peaks (0.41 ± 0.02 nA versus 0.33 ± 0.03 nA, $p < 0.0001$, paired t-test), and their troughs were shorter in duration (3.9 ± 4.4 ms versus 30.3 ± 8.6 ms, $p < 0.0001$) and less negative (minimum values of –0.04 ± 0.02 versus –0.09 ± 0.01, $p < 0.0001$).

The features of the ACTs calculated from different subsets of interspike intervals can be related to changes in the distance to spike threshold during the interspike interval. The hazard rate (see METHODS) provides an estimate of the relative distance to threshold as a function of time since the previous spike (Matthews 1996; Powers & Binder 2000). Due to the afterhyperpolarization (AHP) following motoneurone spikes, the distance to threshold is large immediately following a spike and the hazard rate is zero or very low. As the AHP decays, the membrane potential rises toward threshold, leading to a progressive increase in the hazard rate. If the mean level of membrane depolarization is below threshold after the AHP has completely decayed, the hazard rate approaches a constant level and spikes are only evoked by positive noise-induced deflections (Matthews 1996; Powers & Binder 2000). For suprathreshold levels of mean depolarization, the membrane potential and the hazard rate increase monotonically after a spike.

Begin small print section

The hazard rate estimates are subject to considerable sampling variability, particularly for the low bin counts typical of the longest interspike intervals (see METHODS and Wetmore & Baker 2004). However, in most cases they provide a good estimate of the relative AHP amplitude as function of time from the previous spike (cf. Fig. 8A in Powers & Binder 2000).

End small print section

Figure 3A and B show ISI histograms and hazard rates calculated from discharge records collected at three different mean firing rates in the same motoneurone ("Low", gray traces: 13.2 imp/s; "Medium", thin black traces: 16.8 imp/s; "High", thick black traces: 20.2 imp/s). For all three mean firing rates, the hazard rates increase for the first 100 ms of the post spike interval, indicating that the membrane potential is steadily approaching threshold during this time. However, the hazard rates at a particular post spike interval increase with increasing mean discharge rate, suggesting that at a particular post spike interval, the distance to threshold decreases with increasing mean rate. Figure 3C – E shows the ACTs calculated separately for two ranges of ISIs (indicated by vertical dashed lines in Fig. 3A and B):

0 – 50 ms (C and D) and 50 – 100 ms (E and F) at each of the three different mean discharge rates for this motoneurone. The ACT calculated for the shorter ISIs at the lowest discharge rate (gray traces in C and D) shows the largest peak and no trough, whereas that calculated for longer ISIs at the highest discharge rate (thick black traces in E and F) shows the smallest peak and the largest and longest trough. These differences simply reflect different requirements for noise-evoked spikes as a function of the membrane potential's distance to threshold. When the distance to threshold is relatively large, spikes can only be evoked with large depolarizing current transients, with no need for preceding hyperpolarization. In contrast, when the membrane potential is close to threshold, longer ISIs can only occur when spikes are delayed by hyperpolarization, after which they can be evoked with relatively small depolarizing current transients.

ACTs calculated from the simulated discharge of two different threshold-crossing neurone models

We used two different threshold-crossing neurone models to explore further the effects of changes in the distance to threshold on ACT features (see METHODS). In both models, the spike threshold was fixed, so that changes in the distance to threshold during the interspike interval were determined solely by changes in the somatic membrane potential. In the standard model, the parameters were adjusted so that the model behavior (i.e., rheobase, input resistance, f-I slope) fell within the range of that observed experimentally. This model included a slow potassium conductance that was incremented by a fixed amount after each spike (threshold-crossing) and then decayed exponentially. This feature gave rise to a simulated AHP similar to that seen in real motoneurones. The second model was identical to the first, except that it had no AHP conductance. To prevent short interspike intervals, this second model has a 10 ms absolute refractory period following a spike, during which time the somatic voltage was set at a level similar to the mean depolarization. The two models were subjected to the same set of noisy current waveforms as used experimentally, and the mean current level was adjusted so that their mean discharge rates were similar to that of the motoneurone shown in Figure 1 (about 17 imp/s).

Figure 4 shows the discharge statistics (A and B), and spike-triggered averages of somatic membrane potential (C and D) and injected current (E and F) for the two models. The behavior of the model with the AHP is shown in the left panels and that of the model without the AHP on the right. The presence of an AHP prevents short interspike intervals and produces relatively regular discharge (coefficient of variation of ISIs (CV) = 0.18). The ISI histogram (Fig. 4A, thin line) is narrow and symmetric, and the hazard rate (Fig. 4A, thick line) exhibits a monotonic rise. These features are similar to those observed in our experimental data (e.g., Figs. 3 and 7), although the model neurone's discharge was more regular. In the absence of an AHP, the same mean rate of discharge is associated with greatly increased variability (CV = 0.81). The ISI histogram is positively skewed with a long, exponential tail, and the hazard rate is relatively constant for intervals longer than the refractory period (Fig. 4B). The difference in the hazard rates for the two models can be related to shape of the average voltage trajectory surrounding spikes. The model with the AHP exhibits a large hyperpolarization following a spike followed by a linear rise toward threshold and a sharp depolarization just prior to the threshold crossing (Fig. 4C). During the period of hyperpolarization, no spikes occur, so that the hazard rate is zero. The linear rise toward threshold is associated with a monotonic increase in the hazard rate. In contrast, the perispike membrane trajectory in the model without the AHP is flat (Fig. 4D), as is the hazard rate.

The ACTs for the two models are shown in the bottom panels of Figure 4. A clear trough about 30 ms in duration is present in the model with the AHP (Fig. 4E), but not in the model without the AHP (Fig. 4F). The peak amplitude of the ACT is smaller in the model with the AHP, reflecting the fact that about 5 ms prior to the spike, the membrane potential is higher in this model than in that without the AHP (arrows in C and D), so that less additional depolarization is required for the model neurone to cross threshold. For both models, there is a decrease in the standard deviation (gray traces in E and F) around the time of the ACT peak, and this decrease is smaller in the model with the AHP

Computer simulations permitted us to generate much larger data sets than we typically collected during the experiments. The simulated spike discharge records analyzed in Figure 4 were based on over

20,000 spikes, whereas the experimental records contained between 1000 and 4000 spikes. These large simulated data sets made it possible to calculate separate ACTs for spikes preceded by more restricted ranges of interspike intervals. Figure 5 shows ACTs calculated separately for spikes preceded by ISIs in 10 ms increments, over the range of ISIs present in both models (30 – 90 ms). Figure 5A and B show ACTs calculated from the discharge of the model with an AHP, whereas Fig. 5C and D illustrate analogous ACTs calculated for the model without an AHP. In both models, all of the ACTs exhibited a large peak immediately preceding the spike, and a smaller peak preceding the spike by the ISI duration used in the analysis. However, the two models differed in terms of the characteristics of the troughs between the peaks and in the relation of the peak amplitude to the ISI duration. For the model without an AHP, the ACTs calculated for all of the illustrated ISI ranges exhibited troughs in between the two peaks, whereas no trough was present for the shortest ISI range for the model with an AHP (bold traces in Fig. 5A and B). The amplitude of the trough was independent of ISI duration in the model without the AHP. In contrast, in the model with an AHP, increasing ISI ranges are associated with a progressive increase in trough amplitude. The amplitude of the peak of the ACT immediately preceding the spike was the same for all ISIs for the model without the AHP, whereas those associated with the model with the AHP exhibit a progressive decrease in the peak immediately preceding the spike with increasing ISI duration.

This analysis shows that in both models, each range of ISIs is associated with a particular average current trajectory. The overall ACT reflects the contribution of all of these trajectories, weighted by the probability of occurrence of different ISIs. The presence of an AHP produces systematic distortions in the shape of the current trajectories associated with different ISIs. As a result, the overall ACT reflects the influence of both stimulus history and discharge history on firing probability.

We compared the behavior of models with and without AHPs to make the contribution of the AHP to the time course of the average ACT obvious; when an AHP is present, so is the ACT trough. However, qualitatively similar changes in the ACT can be achieved by changing the time course of the

AHP. We performed additional simulations in which we varied the time constant of the AHP decay and kept the mean rate constant by changing the D.C. current level. Reducing the AHP time constant led to a decrease in the amplitude of the trough, whereas increasing the AHP time constant had the opposite effect (data not shown).

Autoregressive-moving-average (ARMA) representation of spike discharge

To obtain distinct estimates of the effects of stimulus history and discharge history on firing probability, we modeled the noise-driven neuronal discharge as an autoregressive moving average (ARMA) process (Box *et al.* 1994; see METHODS). In this model, the relation between spike probability and stimulus input is predicted based on a stimulus kernel (moving average component) and a feedback kernel (autoregressive component). In other words, the probability of spike occurrence at a given point in time depends both on the history of the stimulus and a feedback term that depends upon the times of occurrence of previous spikes. Each kernel is specified by a list of coefficients specifying its amplitude (i.e., predicted firing rate) at a particular time lag. The stimulus kernel predicts the average change in firing rate following a stimulus pulse, whereas the feedback kernel predicts the average change in firing rate following an output pulse (i.e., a spike). The estimated values of the coefficients are obtained by minimizing the squared error between the predicted and measured spike output (see METHODS).

Figure 6A shows the stimulus and feedback kernels estimated from the discharge records of a motoneurone firing at three different mean rates (”Low”, gray: 13.2 imp/s; “Medium”, thin black: 16.8 imp/s; and “High”, thick black: 20.2 imp/s, same records as those used for Fig. 3). The stimulus kernels have been normalized based on the lower sampling rate used for the ARMA calculations (0.4 ms, see METHODS), so that the kernel indicates the expected change in firing rate following a 1 nA, 0.4 ms current pulse. These kernels are monophasic, with a sharp peak near time zero followed by an exponential decay to baseline within 5 - 10 ms (see inset in Fig. 6A). The feedback kernels indicate the

expected change in firing rate following an output spike. They show a sharp drop in predicted firing rate following a spike followed by a long return to baseline ($\geq$100 ms) that often exhibits one or more oscillations with a period equal to the mean interspike interval.

The area under the kernels indicates the expected increase or decrease in the number of spikes compared to the background probability following a pulse of current (stimulus kernel) or an output spike (feedback kernel). At the lowest discharge rate, 1.8 fewer spikes are predicted following an output spike whereas a pulse of current leads to an increase in the expected number of spikes of only 0.08. Thus, the occurrence of an output spike clearly has a more pronounced effect on discharge probability than does a brief, pulse of current. The characteristics of both kernels depend upon mean discharge rate. The time course of the feedback kernel clearly changes with mean firing rate, whereas the stimulus kernels calculated at different discharge rates are quite similar in shape. However, the areas of both the stimulus kernels and the feedback kernels increase with mean discharge rate. For the discharge records used in Figure 6, the stimulus kernel areas were 0.08, 0.09 and 0.10 impulses at the low, medium and high discharge rates and those of the feedback kernels were –1.84, -2.55 and –4.43 impulses. For all cases in which kernel areas could be compared at different discharge rates in a given cell, both the stimulus and feedback kernel areas were significantly larger at the higher discharge rate ($p < 0.05$, paired t-test, n=5).

Although the size and duration of the feedback kernel indicates a profound effect of previous discharge on firing probability, the inclusion of this kernel in the model has relatively subtle effects on the time course of the stimulus kernel. If spike output is predicted solely on the basis of stimulus history, the resultant first-order Wiener kernel estimates are very similar to the stimulus kernels calculated on the basis of the ARMA model. Figure 6B shows the difference in stimulus kernels estimated with and without inclusion of the feedback kernel in the model fit. The difference between these two estimates is a monophasic trough with a duration of about 40 ms and an amplitude that increases with increasing mean discharge rate. Since the first-order Wiener kernel is a time-reversed, scaled version of the

average current trajectory (Bryant & Segundo, 1976; Poliakov *et al.* 1997), this analysis supports the idea that the troughs seen in the average current trajectories reflect the effects of the previous spike.

Effects of changes in the AHP on the stimulus and feedback kernels

The decrease in firing probability measured by the feedback kernel is likely to represent the effect of the post spike afterhyperpolarization (AHP). Consequently, changes in the AHP should be reflected as changes in the feedback kernel, even if the mean discharge rate is held constant. We tested this prediction by adding 1 mM TEA to the extracellular solution. Previous work suggests that this concentration of TEA increases the AHP by producing a partial block of the delayed rectifier potassium conductance, which in turn leads to an increase in spike width, increased calcium influx and increased activation of the SK-type calcium-activated potassium conductance (Viana *et al.* 1993). We measured the effect of TEA on the AHP by comparing spike-triggered averages of the membrane potential during noise-driven discharge at similar mean rates in control conditions and following the addition of TEA. Spike width was increased in all cases (n=9) and in most cases (6/9) this led to an increase in the amplitude of the AHP. The effect of TEA is illustrated in Figure 7A, which shows spike-triggered averages of the membrane potential during noise-driven discharge before ("Control", thin black), during ("TEA", thick black) and after TEA application ("Wash", gray). The application of TEA produced two main effects on motoneurone discharge. First, the slope of the steady-state frequency-current relation (f/I) was significantly decreased in TEA (10.4 ± 2.4 imp/s/nA vs. 17.4 ± 5.8 imp/s/nA in control; $p < 0.05$, paired t-test, n=6). Second, for matched mean discharge rates, ISI variability during noise-driven discharge was significantly reduced in TEA (coefficient of variation = 0.19 ± 0.08 vs. 0.29 ± 0.10 in control, $p < 0.0001$, n=9). Figure 7B and C illustrate the effect of TEA on discharge statistics. The interspike interval histograms before ("Control", thin black) and after TEA ("Wash", gray) are wider than those obtained during TEA ("TEA", thick black). The effects of TEA on the ISI histogram are reflected in a more steeply rising hazard rate than seen in control conditions.

Figure 7D illustrates the stimulus (upper traces) and feedback kernels (lower traces) estimated from noise-driven discharge before, during and after TEA application. The feedback kernel increases in amplitude during TEA, reflecting a more pronounced drop in firing probability resulting from the increased AHP. When compared at matched discharge rates, the areas under the feedback kernels during TEA were significantly greater than those measured under control conditions (paired t-test, $p < 0.001$ n=9), and were on average 144 % (± 23%) of the areas measured during control conditions. Noise-driven discharge at the same mean rate was obtained before, during and after TEA application in three cases. In each case, the feedback kernel recovered to near control values (100 ± 14%) after TEA was washed out. The area under the stimulus kernel was reduced during TEA application to 87 ± 5% of the control area, and this difference was significant ($p < 0.001$, paired t-test, n=9). However, a similar reduction was seen following TEA washout (93 ± 8% of control), so it is not clear if this represents a specific effect of TEA. In any case, the predominant effect of TEA was to increase the amplitude of the feedback kernel, consistent with its effects on AHP amplitude and discharge statistics.

Predicted firing rate changes based on the ARMA kernels and the first-order Wiener kernel

The stimulus and feedback kernels (and the first-order Wiener kernel alone) can be used to predict the effect of current transients on firing rate. We embedded Poisson trains of positive and negative alpha function transients in our noisy current stimulus in order to test the predictions of the ARMA model (see METHODS and Poliakov *et al*. 1997). We first compiled peristimulus time histograms (PSTHs) based on the relation between the times of spike occurrence and the times of occurrence of the positive and negative alpha functions. The black traces in Figure 8 illustrate the PSTHs compiled for symmetric positive (A) and negative (B) transients. The positive current transient produces a brief increase in discharge rate followed by a smaller, more prolonged decrease below the baseline firing rate (indicated by the horizontal dotted line). The negative current transient produces the opposite sequence

of firing rate changes, although the initial decrease in firing rate is significantly smaller than the increase produced by the depolarizing transient.

The sequence of firing rate changes produced by the current transients are composed of a direct effect of the current on the probability of spike occurrence together with the effect of that change in firing probability on the probability of subsequent spikes. The green traces in Fig. 8A and B show the predicted direct effects of the current transients, estimated by convolving the current transients with the stimulus kernel. The predicted effects are short lasting and monophasic, consisting of a rapid change in firing probability followed by an exponential return to baseline. The blue traces show the effects of the cell's discharge history predicted from the feedback kernels. The direct effect of the depolarizing transient is an increase in firing probability above baseline. This increase in discharge leads to a subsequent decrease in firing probability, reflecting the influence of the feedback kernel. The predicted decrease in firing probability slowly returns to baseline and is followed by a slight increase in discharge at a latency approximating the mean interspike interval. The feedback kernel predicts the opposite sequence of firing rate changes following a hyperpolarizing current transient.

The predictions of the full ARMA model, i.e., the sum of the rate changes predicted by the stimulus and feedback kernels, are shown in the red traces. The model predictions provide a good fit to the PSTHs starting at about 5 ms after the onset of the current transient. However, the short-latency PSTH effects are not well predicted by the ARMA model. The model underestimates the increase in firing probability produced by a depolarizing input and overestimates the decrease in firing probability produced by a hyperpolarizing input. These systematic errors are similar to those previously reported for the first-order Wiener kernel (Poliakov *et al.* 1997). In fact, the predictions based on the first-order Wiener kernel (not shown) are virtually identical to those shown for the ARMA model. These findings are thus consistent with the representation of the motoneurone output as a cascade of a linear filter followed by a static nonlinearity (Poliakov *et al.* 1997; Binder *et al*. 1999). The present results show that

the characteristics of the initial, linear filter estimated from the first-order Wiener kernel reflect a combination of the effects of stimulus and discharge history.

DISCUSSION

The average current-trajectory (ACT) preceding spikes in noise-driven neuronal discharge reveals the features of the input that are most relevant in the spike-triggering process (Bryant & Segundo, 1976; Mainen & Sejnowski, 1995; Aguera y Arcas *et al*. 2003). The time course of the ACT is thought to reflect the influence of the current-induced changes in membrane potential on activation or inactivation of voltage-dependent conductances (Mainen & Sejnowski, 1995; Poliakov *et al*. 1997; Binder *et al*. 1999; Fellous *et al*. 2003; Gutkin *et al*. 2003; Svirskis *et al*. 2002, 2004). The results of the present study demonstrate that the time course of the ACT (and the related first-order Wiener kernel) reflects a combination of the effects of the stimulus current and recent discharge history on firing probability. The effects of discharge history are likely to be largely mediated by the calcium-activated potassium conductance underlying the post spike afterhyperpolarization (AHP).

Dependence of ACT features on the length of the preceding interspike interval

We computed ACTs first by averaging the current preceding all spikes from several epochs of noise-driven discharge exhibiting similar mean discharge rates. As previously reported (Bryant & Segundo, 1976; Mainen & Sejnowski 1995; Poliakov *et al.* 1997; Binder *et al*. 1999; Svirskis *et al.* 2002, 2004), ACTs were characterized by a shallow hyperpolarizing trough followed by a sharp depolarizing peak just prior to spike onset. We then computed ACTs based on subsets of interspike intervals and found that the hyperpolarizing trough of the ACT was present for average trajectories triggered by spikes whose preceding interspike interval was longer than the median, but not for those triggered by spikes preceded by interspike intervals shorter than the median value. Qualitatively similar ACTs could be

elicited in a simple threshold-crossing model with an exponentially decaying post-spike potassium conductance without an explicit representation of the currents underlying action potentials. These findings suggest that the hyperpolarizing trough in the ACT does not necessarily reflect the removal of sodium inactivation as previously proposed (Mainen & Sejnowski, 1995; Poliakov *et al*. 1997; Fellous *et al*. 2003; Gutkin *et al*. 2003; Svirskis *et al*. 2002, 2004). We suggest instead that the combination of the mean injected current and the calcium-activated potassium current underlying the post-spike afterhyperpolarization (AHP) produces a voltage trajectory that tends to cross threshold at the mean interspike interval. Longer intervals can only be produced when the current trajectory drops below the mean value to prevent threshold crossing. Further support for this interpretation comes from the finding that ACTs computed from the discharge of a threshold-crossing model without an AHP did not show a hyperpolarizing trough. Although our experimental and modeling results do not exclude the possibility that sodium channel inactivation contributes to the trough the ACT, they suggest that for any neurone exhibiting prolonged post-spike changes in conductance, previous discharge history will make a prominent contribution to the ACT trough. This effect may be particularly strong in motoneurones, which exhibit large AHPs and relatively low interspike interval variability (Matthews 1996; Powers & Binder 2000). However, similar calcium-mediated AHPs are present in a variety of central neurones (cf. Sah 1996).

We used threshold-crossing neurone models with and without an AHP to generate a sufficient number of spikes to examine in more detail the average stimulus features associated with different interspike intervals. These features are easiest to interpret in the threshold-crossing model without an AHP. Following a spike in this model, the membrane voltage was set to a level near the mean level of membrane potential for a short (10 ms) absolute refractory period, after which the membrane potential was determined by the sum of the stimulus and leak currents. As a result, the average membrane trajectory between spikes was flat (Fig. 4D), as was the probability of spike occurrence (i.e., the hazard rate) for intervals longer than the absolute refractory period (Fig. 4B, thick line). As the distance to

threshold does not vary during the interspike interval in this model, the ACTs associated with all interspike intervals are characterized by a stereotyped depolarizing peak prior to spike onset (Fig. 5C and D). Not surprisingly, this peak is preceded by another, smaller peak at the duration of the interspike interval (Fig. 5C). These peaks are separated by a trough of constant amplitude, indicating that the generation of a particular interspike interval requires hyperpolarization to prevent spike occurrence in addition to the depolarizing current transient to elicit spikes at the specified times. The occurrence of an AHP following a spike produces systematic distortions in the ACTs that differ according to interspike interval. The occurrence of short interspike intervals now does not require hyperpolarizing stimulus current, since the requisite hyperpolarization is supplied by the AHP current. The generation of interspike intervals of increasing length requires a progressive increase in the hyperpolarizing trough in the ACT to compensate for the decay of the AHP current. The size of the depolarizing peak in the ACT also varies systematically with the interspike interval. As the time from the previous spike increases, the membrane potential approaches threshold (Fig. 4C), so longer intervals require less stimulus-induced depolarization to reach threshold than do shorter intervals (Fig. 5A and B).

The ACT calculated from all spikes at a given mean discharge rate reflects the contribution of the current trajectories associated with particular interspike intervals, weighted by their probability of occurrence (see also Aguera y Arcas & Fairhall 2003; Pillow & Simoncelli 2003). The interspike interval distribution itself reflects the influence of the AHP on discharge probability (Matthews, 1996; Powers & Binder, 2000). Thus the ACT and the related first-order Wiener kernel reflect the influence of both stimulus and discharge history on firing probability.

Calculation of separate kernels reflecting the influence of stimulus history and discharge history

To separate the effects of discharge and stimulus history on spike probability, we modeled the spike train as an autoregressive-moving average (ARMA) process (Box *et al.* 1994), in which the effects of discharge history are represented by an autoregressive (AR, feedback) kernel and the effects of stimulus

history by a moving average (MA, stimulus) kernel. The feedback kernels predicted a prolonged (~ 100 ms) decrease in firing rate following a spike. The stimulus kernels predicted a much briefer (~ 5 ms) increase in rate following a pulse of stimulus current, without the subsequent decrease in firing rate predicted by the standard first-order Wiener kernel. The amplitude of both kernels increased with increasing firing rate. Enhancement of the AHP current in the neurones by adding TEA to the bathing solution led to a pronounced increase in the amplitude of the feedback kernel but relatively minor effects on the stimulus kernel.

A number of other models have been proposed that predict firing probability as a function of both the stimulus history and discharge history, i.e., the recovery of excitability as a function of time since the previous spike. These include expressing the firing probability as the sum of stimulus and recovery-related functions as in our approach (Joeken *et al*. 1997; Kistler *et al*. 1997; Keat *et al.* 2001; Pillow *et al*. 2004) and as a product of these two functions (Gaumond *et al*. 1982; Berry & Meister, 1998; Miller & Wang, 1993; Schmich & Miller, 1997). In most cases, these models either assume a recovery function with a fixed time course (e.g., Berry & Meister, 1998; Keat *et al.* 2001), or are based on an explicit model of spike generation (e.g., Kistler *et al*. 1997; Pillow *et al*. 2004). In contrast, our ARMA characterization of spike generation shows that the amplitude and time course of post spike recovery (as estimated feedback kernel) changes with mean firing rate (Fig. 6) and can be altered by manipulating the conductance underlying the medium AHP (Fig. 7).

Joeken and colleagues (1997) used an approach very similar to ours to model the discharge of pigeon auditory nerve fibers. However, the results of their analysis differed from ours in two important respects. First, their feedback kernels were relatively short lasting (returning to baseline with 10 ms) and often exhibited a positive overshoot. In addition, they reported that the stimulus kernel estimated from the model that included the feedback kernel did not differ significantly from the first-order Wiener kernel, whereas the stimulus and first-order Wiener kernels that we calculated showed small but systematic differences that changed as function of mean firing rate (Fig. 6B). The differences between

our results and those of Joeken *et al.* (1997) may simply reflect the fact that auditory nerve fibers exhibit a relatively rapid recovery of excitability following a spike.

Predictions based on the ARMA coefficients and the first-order Wiener kernel

We have also shown that the linear prediction of current-evoked changes in firing probability based on the first-order Wiener kernel represents the sum of the predicted changes based on the AR and MA kernels. As a result, the predictions of the ARMA model exhibit the same systematic deviations from the observed changes in firing probability as previously reported for those based on the first-order Wiener kernel (Poliakov *et al*. 1997). Both predictions underestimate the increase in firing probability produced by a depolarizing input and overestimate the decrease produced by a hyperpolarizing input. These systematic deviations are consistent with the presence of a nonlinear element (Poliakov *et al*. 1997). Previous analyses have suggested that the process of spike initiation can be represented by "Wiener cascade" or "LN model" in which the initial linear filter is followed by a static nonlinearity (Hunter & Korenberg, 1986; Berry & Meister 1996; Poliakov *et al*. 1997; Binder *et al*. 1999). Although our results show that the linear filter (i.e., the first-order Wiener kernel) already incorporates the effects of discharge history, a closer correspondence between model parameters and the underlying biophysics mechanisms can be obtained by placing the feedback element after the nonlinearity (Keat *et al*. 2001). Thus, the initial linear filter may represent the effects of the stimulus on membrane voltage as mediated by the passive electrical properties of the cell and voltage-gated conductances activated in the subthreshold range. The existence of a voltage threshold for spike initiation introduces the nonlinear element, and the additional conductances activated by the spike constitute the feedback element.

Functional implications

The recent explosion of interest in deciphering the 'neural code' (e.g., Abeles, 1991; Shadlen & Newsome, 1994; Rieke *et al*. 1996) has led to a renewed appreciation of the ACT as an important

measure of how neurones respond to the dynamic aspects of synaptic current (Mainen & Sejnowski, 1995; Svirskis *et al*. 2002,2004; Svirskis & Rinzel 2003). In particular, the duration of the ACT peak influences the precision of spike timing (Mainen & Sejnowski, 1995) and also indicates the time window over which coincident synaptic inputs trigger spikes most effectively (Svirskis *et al*. 2004). Also, the presence of a hyperpolarizing trough in the ACT has been interpreted as indicating that certain combinations of synaptic input (i.e., an IPSP followed by an EPSP) result in enhanced spike generation in the postsynaptic neurone (Gutkin *et al*. 2003; Svirskis *et al*. 2004). Although there has been some recent interest in the role of slow potassium conductances (including a calcium-activated potassium conductance) in determining spike timing reliability (Schreiber *et al*. 2004), most explanations of the biophysical mechanisms underlying ACT features have focused on the role of voltage-activated subthreshold conductances (Gutkin *et al*. 2003; Svirskis *et al*. 2002, 2004). However, the present results clearly indicate that shape of the ACT is strongly influenced by the calcium-activated potassium conductance underlying the AHP.

REFERENCES

Abeles M (1990). Corticonics: Neural Circuits of the Cerebral Cortex. Cambridge University Press, Cambridge, UK.

Aguera y Arcas B & Fairhall AL (2003). What causes a neuron to spike? *Neural Comput* **15**, 1789-1807.

Aguera y Arcas B, Fairhall AL & Bialek, W (2003). Computation in a single neuron: Hodgkin and Huxley revisited. *Neural Comput* **15**, 1715-1749.

Berry MJ & Meister M (1998). Refractoriness and neural precision. *J Neurosci* **18**, 2200-2211.

Binder MD, Poliakov A &Powers RK (1999). Functional identification of input-output transforms of mammalian motoneurones. *J Physiol (Paris)* **93**, 29-42.

Box, GEP, Jenkins GM & Reinsel GC (1994). *Time Series Analysis: Forecasting and Control*. 3rd ed. Prentice Hall, New York.

Bryant HL & Segundo JP (1976). Spike initiation by transmembrane current: a white-noise analysis. *J Physiol* **260**, 279-314.

de Boer E & Kuyper, P (1968). Triggered correlation. *IEEE Trans Biomed Engr* **15**, 169-179.

Draper NR & Smith, H (1998). Applied Regression Analysis. Third Ed. New York: Wiley-Interscience.

Fellous JM, Rudolph M, Destexhe A & Sejnowski TJ (2003). Synaptic background noise controls the input/output characteristics of single cells in an in vitro model of in vivo activity. *Neurosci* **122**, 811-829.

Gaumond RP, Molnar CE & Kim DO (1982). Stimulus and recovery dependence of cat cochlear nerve fiber spike discharge probability. *J Neurophysiol* **48**, 856-873.

Gutkin B, Ermentrout GB & Rudolph M (2003). Spike generating dynamics and the conditions for spike-time precision in cortical neurons. *J Comput Neurosci* **15**, 91-103.

Hunter IW & Korenberg MJ (1986). The identification of nonlinear biological systems: Wiener and

Hammerstein cascade models. *Biol Cybern* **55**, 135-144.

Joeken S, Schwegler H & Richter CP (1997). Modeling stochastic spike train responses of neurons: an extended Wiener series analysis of pigeon auditory nerve fibers. *Biol Cybern* **76**, 153-162.

Keat J, Reinagel P, Reid RC & Meister M (2001). Predicting every spike: a model for the responses of visual neurons. *Neuron* **30**, 803-817.

Kistler WM, Gerstner W & Leo van Hemmen J (1997). Reduction of the Hodgkin-Huxley equations to a single-variable threshold model. *Neural Computation* **9**, 1015-1045.

Mainen ZF & Sejnowski, TJ (1995). Reliability of spike timing in neocortical neurons. *Science* **268**, 1503-1506.

Matthews PBC (1996). Relationship of firing intervals of human motor units to the trajectory of post-spike after-hyperpolarization and synaptic noise. *J Physiol* **492**, 597-628.

Miller MI & Wang J (1993). A new stochastic model for auditory-nerve discharge. *J Acoust Soc Am* **94**, 2093-2107.

Paarmann LD & Korenberg MJ (1992). Estimation of parameters of an ARMA signal model based on orthogonal search. *IEEE Transactions on Automatic Control* **37**, 347-352.

Pillow J & Simoncelli EP (2003). Biases in white noise analysis due to non-Poisson spike generation. In *Neurocomputing* Vol. **52-54**, 109-115, Elsevier.

Pillow J, Paninski L & Simoncelli E. (2004). Maximum likelihood estimation of a stochastic integrate-and-fire neural model. In S. Thrun, L. Saul and B. Scholkopf (eds.). Advances in Neural Information Processing Systems. Cambridge, MA: MIT Press, pp. in press.

Poliakov AV, Powers RK & Binder, MD (1997). Functional identification of the input-output transforms of motoneurones in the rat and cat. *J Physiol* **504**, 401-424.

Powers RK & Binder, MD (2000). Relationship between the time course of the afterhyperpolarization and discharge variability in cat spinal motoneurones. *J Physiol* **528**, 131-150.

Press WH, Flannery BP, Teukolsky SA & Vetterling WT (1992). Numerical Recipes: The Art of

Scientific Computing. Second ed. Cambridge, U.K.: Cambridge University Press.

Rieke F, Warland, D, van Steveninck, R & Bialek, W. (1996). *Spikes: Exploring the Neural Code*. Cambridge, Massachusetts: MIT Press.

Sah P (1996). Ca2+-activated K+ currents in neurones: Types, physiological roles and modulation. *Trends in Neurosci* **19**, 150-154.

Sawczuk A, Powers RK & Binder, MD (1995). Spike frequency adaptation studied in hypoglossal motoneurons of the rat. *J Neurophysiol* **73**, 1799-1810.

Sawczuk A, Powers RK & Binder MD (1997). Contribution of outward currents to spike-frequency adaptation in hypoglossal motoneurons of the rat. *J Neurophysiol* **78**, 2246-2253.

Schreiber S, Fellous JM, Tiesinga P & Sejnowski TJ (2004). Influence of ionic conductances on spike timing reliability of cortical neurons for suprathreshold rhythmic inputs. *J Neurophysiol* **91**, 194-205.

Schmich RM & Miller MI (1997). Stochastic threshold characterization of the intensity of active channel dynamical action potential generation. *J Neurophysiol* **78**, 2616-2630.

Shadlen MN & Newsome WT (1994). Noise, neural codes and cortical organization. *Cur Opin Neurobiol* **4**, 569-579.

Svirskis G, Kotak V, Sanes D & Rinzel, J (2004). Sodium along with low threshold potassium currents enhance coincidence detection of subthreshold noisy signals in MSO neurons. *J Neurophysiol* **91,** 2465 - 2473

Svirskis G, Kotak V, Sanes DH & Rinzel J (2002). Enhancement of signal-to-noise ratio and phase locking for small inputs by a low-threshold outward current in auditory neurons. *J Neurosci* **22**, 11019-11025.

Svirskis G & Rinzel, J (2003). Influence of subthreshold nonlinearities on signal-to-noise ratio and timing precision for small signals in neurons: minimal model analysis. *Network* **14**, 137-150.

Viana F, Bayliss DA & Berger AJ (1993). Multiple potassium conductances and their role in action

potential repolarization and repetitive firing behavior of neonatal rat hypoglossal motoneurons. *J Neurophysiol* **69**, 2150-2163.

Viana F, Gibbs L & Berger AJ (1990). Double- and triple-labeling of functionally characterized central neurons projecting to peripheral targets studied *in vitro*. *Neurosci* **38**, 829-841.

Wetmore DZ, & Baker SN (2004). Post-spike distance-to-threshold trajectories of neurones in monkey motor cortex. *J Physiol* **555**: 831-850.

ACKNOWLEDGEMENTS

We thank Mr. Paul Newman for technical assistance throughout the project. This work was supported by Grants NS-26840 and NS-31925 from the National Institute of Neurological Disorders and Stroke and Grant IBN-9986167 from the National Science Foundation.

APPENDIX

Bryant and Segundo (1976) suggested modeling a nerve firing process using Wiener kernels (see their equations (6) through (8)). In the context of our notation, the first order model is

$$Y_n - \mu = \sum_{j=1}^{q} a_j X_{n-j}$$

Here Y_n is one (zero) if a firing occurred (did not occur) during the nth time interval; μ is the average of the sequence Y_n with respect to n; the a_j's are moving average coefficients; and X_n is the input stimulus during the nth interval. Higher order Wiener kernels have also been used to model nerve firings (Poliakov et al. 1997). These models extend the above by including linear combinations of products of the stimulus at various times. By contrast, we consider the following extension:

$$Z_n = \sum_{j=1}^{q} a_j X_{n-j} + \sum_{j=1}^{p} b_j Z_{n-j} + R_n$$

where $Z_n = Y_n - \mu$; the b_j's are the autoregressive coefficients; and R_n is an error term. For convenience, we refer to the above as an autoregressive/moving average (ARMA) model, but, for a true ARMA model, we would need to set R_n to X_n.

The models that we consider have large values for p and q so that we can take into account many previous time points. There are many different methods for estimating the coefficients in high order ARMA models but these methods assume that observations of X_n are not available (see, e.g., Paarmann & Korenberg 1992 and references therein).

The method that we consider here starts with the usual least squares approach of finding a_j's and b_j's that minimize the sum of the squared residuals, i.e., R_n^2. In other words, the least squares approach determines the coefficients a_j and b_j by minimizing the following function:

$$F(a,b) = \frac{1}{2N} \sum_{n=1+\max(p,q)}^{N} \left[Z_n - \sum_{j=1}^{q} a_j X_{n-j} - \sum_{j=1}^{p} b_j Z_{n-j} \right]^2$$

where N is the total number of time points.

We estimate the a_j and b_j coefficients using a slight modification of the least squares approach, together with a new numerical procedure. The basic idea is to include some extra terms in our objective function so that the solution of the linear least squares problem can be found by inverting a Toeplitz matrix. Once this is accomplished, we use Rybicki's method for solving a non-symmetric Toeplitz system (as documented in Section 2.8 of Press et al. 1992). To be specific, our modified objective function is

$$G(a,b) = \frac{1}{2N} \sum_{n=1}^{N} \left[Z_n - \sum_{j=1}^{q} a_j X_{n-j} - \sum_{j=1}^{p} b_j Z_{n-j} \right]^2$$

For the cases where $n - j < 1$ in the equation above, X_{n-j} is interpreted as X_{N+n-j} and Z_{n-j} is interpreted as Z_{N+n-j}.

Since both the original and modified minimization problems are linear least squares problems, we can find the solution by solving for where all the partial derivatives are zero. Differentiating F and G with respect to a_i we obtain the following

$$\frac{\partial F}{\partial a_i}(a,b) = \frac{1}{N}\sum_{n=1+\max(p,q)}^{N}\left[Z_n - \sum_{j=1}^{q} a_j X_{n-j} - \sum_{j=1}^{p} b_j Z_{n-j} \right] X_{n-i}$$

$$\frac{\partial G}{\partial a_i}(a,b) = \frac{1}{N}\sum_{n=1}^{N}\left[Z_n - \sum_{j=1}^{q} a_j X_{n-j} - \sum_{j=1}^{p} b_j Z_{n-j} \right] X_{n-i}$$

Setting the derivative equal to zero, the corresponding linear equations for minimizing G are

$$\frac{1}{N}\sum_{n=1}^{N} Z_n X_{n-i} = \sum_{j=1}^{q} a_j \left(\frac{1}{N}\sum_{n=1}^{N} X_{n-j} X_{n-i} \right) + \sum_{j=1}^{p} b_j \left(\frac{1}{N}\sum_{n=1}^{N} Z_{n-j} X_{n-i} \right)$$

where this equation holds for $i = 1,\ldots,q$. We note that, under mild assumptions, as $N \to \infty$ we have

$$\frac{1}{N}\sum_{n=1}^{N} Z_n X_{n-i} \to E\left[Z_n X_{n-i} \right]$$

$$\frac{1}{N}\sum_{n=1}^{N} X_{n-j} X_{n-i} \to E\left[X_n X_{n+j-i} \right]$$

$$\frac{1}{N}\sum_{n=1}^{N} Z_{n-j} X_{n-i} \to E\left[Z_n X_{n+j-i} \right]$$

where E denotes expected value. Taking the partials with respect to b_i leads to another p similar equations with similar limiting values. We also note that the coefficients in the linear equation corresponding to minimizing F have the same limiting values as for minimizing G. In summary, for N large relative to $\max(p,q)$, the minimizers of G are close to the minimizers of F.

We complete the discussion of our method by showing how G can be minimized by the solution of multiple sets of Toeplitz equations. We begin with a Bender's decomposition; to be specific, we fix an initial estimate for $b = (b_1,\ldots,b_p)$ which we denote by b^0 and solve the following equations for $a = (a_1,\ldots,a_q)$:

$$\sum_{j=1}^{q} a_j \left(\sum_{n=1}^{N} X_n X_{n+j-i} \right) = \sum_{n=1}^{N} Z_n X_{n-i} - \sum_{j=1}^{p} b_j \left(\sum_{n=1}^{N} Z_n X_{n+j-i} \right) \quad \text{(A1)}$$

for $i = 1,\ldots,q$. We define the matrix $T \notin \Re^{q\times q}$ and $r \in \Re^{q}$ by

$$T_{i,j} = \sum_{n=1}^{N} X_n X_{n+j-i}$$

$$r_i = \sum_{n=1}^{N}\left(Z_n X_{n-i} - \sum_{j=1}^{p} b_j^0 Z_n X_{n+j-i} \right)$$

It follows that equation (A1) for $i = 1,\ldots,q$ can be written as

$$Ta = r$$

We define the vector $v = \in \Re^{2q-1}$

$$v_k = \sum_{n=1}^{N} X_n X_{n+k}$$

for $k = -q+1,\ldots,q-1$. It follows that $T_{i,j} = v_{j-i}$ and hence T is a Toeplitz matrix (see equation (2.8.8) of Press et al. 1992). Hence we can minimize $F(a, b^0)$ with respect to a by solving a Toeplitz system of linear equations (we refer to that solution as a^1). A similar analysis leads to the conclusion that given a^1, we can minimize $F(a^1, b)$ with respect to b by solving a similar Toeplitz system (we refer to that solution as b^1). Thus, we alternate between a and b to obtain a sequence of iterates (a^k, b^k) that converge to the minimizer of $F(a,b)$ with respect to both a and b.

FIGURE LEGENDS

Figure 1. A. Average spike-evoking current trajectory (ACT, lower, thick black trace, left axis) and standard deviation about the average current (upper, gray trace, right axis). The traces were computed from nine trials of noise-driven discharge of a rat hypoglossal motoneurone firing at a mean rate of 17.1 imp/s (for a total of 4011 spikes). The lower set of dashed lines show the 98% confidence limits for the average trajectory and the upper dashed lines show the 98% confidence limits for the standard deviation. The lower two arrows indicate the duration of the trough in the ACT and the upper arrow indicates the point at which the standard deviation drops consistently below the 98% limits. **B.** Same as **A**, at an expanded time scale.

Figure 2. A. ACTs calculated for all intervals (thick black traces), intervals shorter than the median interval ("Short", gray traces) and intervals longer than the median ("Long", thin black traces). **B.** Same as **A**, with an expanded time scale.

Figure 3. Comparisons of ACTs calculated for the same range of interspike intervals at different mean discharge rates. **A.** Interspike interval (ISI) histograms compiled from the records of noise-driven discharge of a single motoneurone firing at mean rates of 13.2 ("Low", gray), 16.8 ("Medium", thin black) and 20.2 ("High", thick black) imp/s. **B.** Hazard rates calculated from ISI histograms in **A**. **C** and **D.** ACTs calculated from spikes preceded by ISIs less than 50 ms. **E** and **F.** ACTs calculated from spikes preceded by ISIs between 50 and 100 ms.

Figure 4. Comparison of the behavior of two threshold-crossing models, one with an AHP conductance (**A**, **C** and **E**), and one without (**B**, **D** and **F**). **A.** and **B**. ISI histograms and hazard rates. **C.** and **D.** Average perispike membrane trajectories. **E.** and **F.** Average and standard deviation of spike-evoking currents.

Figure 5. Average current trajectories (ACTs) calculated for spikes associated with different durations of the preceding interspike interval (ISI). **A.** and **B.** ACTs for the model with an AHP. **C.** and **D.** ACTs for the model without an AHP. The bold traces are ACTs calculated for the shortest ISIs and the gray traces are those calculated for the longest ISIs.

Figure 6. **A.** Stimulus (upper traces) and feedback kernels (lower traces) calculated from discharge records at three different discharge rates (same records as those used in Fig. 3). Bold traces are kernels for the highest discharge rates and gray traces for those at the lowest discharge rates. The inset shows the first 20 ms of the stimulus kernels. The stimulus kernels are very similar at all three discharge rates. **B.** The difference between stimulus kernels and the first-order Wiener kernels.

Figure 7. Effects of 1 mM TEA on interspike voltage-trajectories, discharge statistics and ARMA kernels. **A.** Spike-triggered averages of membrane potential during noise-driven discharge in control (thin black traces), TEA (thick black) and washout (gray traces). **B.** and **C**. Interspike interval histograms and hazard rates for control, TEA and wash. **D.** Wiener kernels (upper traces) and feedback kernels (lower traces) for control, TEA and wash. Inset shows Wiener kernels on expanded time scale.

Figure 8. Predicted and measured effects of depolarizing **(A)** and hyperpolarizing **(B)** current transients on firing probability. The measured effects are represented by the peristimulus time histograms (PSTHs, in black). Predictions are based on the feedback kernel alone (blue traces), the Wiener kernel alone (green traces) or the sum of the two predictions (red traces). Insets show expanded versions of the initial changes in firing probability along with the predicted changes. Calibration bars are 10 imp/s and 2 ms.

Response to Reviewer 1.

I have one major comment, which can readily be addressed by the authors. As pointed out in the present ms, the issues related to the neural code include those of neural synchrony, and precise timing of discharge. However the cells investigated here are motoneurones: for most circumstances precise timing of spikes is unimportant for motoneurone function. This is certainly true for the circumstance set up by the authors here, steady firing under the influence of steady currents, where it is universally recognised that the AHP is the prime regulator of the discharge. However, for the cells for which the alternative interpretations have been put forward (cortical or sensory neurones) this is unlikely to be the case. In fact the authors go a little part of the way to admitting this at the end of the second para of Discussion, by pointing out, as logic demands, that, by their showing of a sufficient mechanism via the AHP to produce a trough in the ACT, they are not ruling out that other mechanisms, such as hyperpolarization to remove sodium channel inactivation, could still contribute. However, they need to go further than this (perhaps by admitting teleology), by pointing out the differences between the firing patterns of motoneurones and the other types of neurones from which the differing ideas have been derived.

We have extended the second paragraph of the DISCUSSION to address the fact that the regular patterns of motoneurone discharge suggest an unusually strong influence of the AHP on the probability of spike occurrence: "Although our experimental and modeling results do not exclude the possibility that sodium channel inactivation contributes to the trough the ACT, they suggest that for any neurone exhibiting prolonged post-spike changes in conductance, previous discharge history will make a prominent contribution to the ACT trough. This effect may be particularly strong in motoneurones, which exhibit large AHPs and relatively low interspike interval variability (Matthews 1996; Powers & Binder 2000). However, similar calcium-mediated AHPs are present in a variety of central neurones (cf. Sah 1996)."

Minor points

1) p.2, second sentence of Introduction. The authors have put "decides" in quotes, but it is still too anthropomorphic for me. The sentence could easily be worded without such a notion.

We have reworded the sentence as follows: "The probability of spike occurrence in the postsynaptic cell depends not only on the amplitude, but also on the time course of the total synaptic current reaching the spike initiation zone."

2) Without reading the main part of the text the summary is rather hard to follow. In particular the vital 7th sentence "However, an alternative explanation …." is particularly obscure. "to delay spike occurrence" is odd (delay compared to what?), as is "this requirement" (very unclear – what requirement?).
3) The same criticism applies to similar wording in the penultimate sentence of para. 2 on p.3. The wording used in the second sentence of para. 3 of the results (p.8 in my version, where p.4 is blank), "Alternatively, this feature could simply reflect …", is much more clear.

We have rewritten the sentences in the SUMMARY and INTRODUCTION using wording similar to that used in the second sentence of paragraph 2 in RESULTS.

Response to Reviewer 2.

...

GENERAL COMMENTS

This manuscript is of interest to people in motor control, particularly those who deal with dynamic firing characteristics of motoneurones. In general, the manuscript was either very readable (some parts) or very difficult in the others. The curves in different figures could not be differentiated, and there are a lot of problems with the accuracy of equations. I hope that the authors will go through their final manuscript with extreme care.

We have redone all of the figures, changing line styles and adding labels to make the different curves more distinct. We have also checked the equations and made the changes requested by the Mathematical Reviewer. We have redone all of the equations using MathType so that the notations are consistent and readable.

SPECIFIC COMMENTS
Summary: Very clear
Introduction: A bit too long but clear

We feel that the all of the material in the INTRODUCTION is needed to explain the rationale for the study and would prefer to retain it.

Methods: Ethics?

We have added a statement in METHODS confirming that all procedures met the appropriate animal welfare guidelines in place at the University of Washington.

Page 5, 2nd paragraph, 5th line from the bottom (correct to ACSF)

Done

Page 5: Stimulus waveform—What is the 42s long injected current waveform? When does the 38 s long step current start after the onset of the 42 s waveform? I assume that 8s after the onset of the step, the white noise and current transients started together.
#(3) not clear.

We now state that the current step started 2 s after the onset of the waveform. The original version had stated that the current transients start at the same as the noise waveform.

Page 5. The equation is not balanced. The factor 1/ô should be unit-less, but ô is not unit-less, therefore 1/ô is not either.

We have corrected this equation as follows:

$$x(i) = (1 - \Delta t / \tau_f) * x(i-1) + gnoise(\sigma) * \sqrt{1 - (1 - \Delta t / \tau_f)^2},$$

Δt and τ_f are both in ms, so their ratio is unit-less.

Page 6: Something is wrong with the first two lines. …filtering time constant was 1 ms (ôf = 10…). I don't get it.

We have corrected this section in accord with the corrected equation. Δt is now given as 0.1 ms and τ_f as 1 ms.

All through the manuscript, when using 2-3 consecutive brackets, could you use {[( )]}, otherwise you make mistakes, and the reader has difficulty reading your equations.

Done

Computer Simulations. What is I in the first equation?

We now state: "I is the current injected into the somatic compartment."

Page 6. Lines 4-6 from the bottom—Not clear. Please re-write both sentences

We have added a parenthetical clause to the last sentence to make the meaning more clear.

Page 7: Lines 5 & 6, and line 10 please take care of the number of opening and closing brackets.

Done

Correct Equation on line 14. Close brackets, move the summing limits where they are supposed to be.

Done

Results
Figures 1,2,3 and the rest : I do not see any bold line or dotted lines.

The line styles were somehow lost in translation from the original figures to the format used in the paper. All of the figures have been redone and saved as pdf files, and the line styles have been changed to gray, thin black and thick black. We have also added labels to further differentiate the different curves.

Page 8: Line 13 from the bottom.. change to "supported"

Done

Page 9: I am not surprised by the results since the two neurones you have used are so different. One is like a motoneurone and the other is not. I am not sure why you used two models, one with AHP and one without. You could have made a stronger case by using two models with different time constants of AHPs. What would happen if you used an S type and an FF type motoneuron? This is not the same as the TEA treated neuron (page 11).

We chose these two models to make the contribution of the AHP to the time course of the average spike-evoking current (ACT) obvious; when an AHP is present, so is the ACT trough. We performed additional simulations in which we varied the time constant of the AHP decay and kept the mean rate constant by changing the D.C. current level. Reducing the AHP time constant led to a decrease in the amplitude of the trough, whereas increasing the AHP time constant had the opposite effect. We have added a paragraph at the end of the RESULTS entitled "**ACTs calculated from the simulated discharge of two different threshold-crossing neurone models**" that presents this analysis**.**

Page 10: ARMA—2nd and 3rd lines from the bottom. It would be better to add another line here translating the kernels to physiology. This part of the manuscript, both in Methods and Appendix, should be translated in terms of physiology. In both these sections, authors have only used mathematical terms without telling a non-mathematical physiologist what it means. This manuscript has been sent to The Journal of Physiology and not Biophysics.

We have expanded this paragraph to clarify the physiological meaning of the ARMA coefficients.

Page 11: Start the first paragraph—"The stimulus (or moving average) kernel reflects the effects of stimulus history, and the feedback (or AR) kernel reflects the discharge history of the neurone." Figure 6A…

Done.

Discussion: No problems, a bit too dry.

Appendix: This really needs to be retyped, there are too many mistakes. It would be nice to see all the vectors (and only the vectors) in bold print. Please relate various terms, where possible, to physiological parameters of your model.

Done

Response to Mathematical Review:

1. Introduction, Page 3, last paragraph: What does it mean to say that "we modeled the spike train as an autoregressive-moving average…"? Does this mean that the ARMA model predicts the times of occurrence of the spikes, which is certainly not the case for the expression given on page 7. It is not clear how this expression would produce a zero or one result for known kernel functions.

We have revised this section of the INTRODUCTION to read as follows: "To separate the effects of discharge history and the stimulus on spike probability, we related the spike train and noisy stimulus via an ARMA model (Box et al. 1994). The effects of discharge history ..." We added the following text, just after "(see Appendix)" which follows the equation for the ARMA model in the Data Analysis section: "The ARMA model relates the spike train and noisy stimulus. It does not predict the zero/one spike train process; rather, any `predictions' made from the model should be interpreted as probabilities or rates of firing. Higher model output values indicate an interval where a spike is more likely to occur." We have also changed 'spike output' to 'spike probability' whenever referring to the predictions of the ARMA model.

2. Stimulus waveform, page 5: There is a conditions of τ_f that must be placed on the expressions for x(i) to prevent it from becoming unbounded. This condition should be given on the same line as the expression.

In the first displayed equation in the Stimulus Waveform section, we have added the following expression to the right of the equation for clarity:

$\tau_f > \Delta t$,

3. Data analysis, Page 6: The expression for the hazard function can only contain definite integrals, which must be made explicit.

The expression now reads: $haz(t) = pdf(t) / (1 - \int_0^t pdf(t)dt)$.

Data analysis, Page 6: The authors appear to use the mean value theorem to arrive at the approximate expression $ln(N_0/N_1)/bw$ for the hazard function, but do not seem to realise that it is a random variable, and that the hazard function estimated by this expression will have a sampling variability. In practice this means that every graph in the text showing the estimated hazard function must also show a confidence interval. This is particularly important in the case of the estimate used in the text. It is not an optimal estimate, and its variance will grow quite rapidly as N_1 becomes small. In the absence of a confidence interval the graphs of the hazard function can not be interpreted. To describe the hazard function over all interspike intervals requires a model for the hazard function, which in this case can be used a s the basis of a maximum-likelihood estimation procedure.

We now acknowledge the issue of sampling variability in the METHODS section. Since we use the hazard function for illustrative purposes rather than statistical comparisons, we do not feel that the addition of confidence intervals is necessary. We also disagree with the reviewer's contention

that the graphs of the hazard function cannot be interpreted. As we now point out in a small print section in the RESULTS section: "The hazard rate estimates are subject to considerable sampling variability, particularly for the low bin counts typical of the longest interspike intervals (see METHODS and Wetmore & Baker 2004). However, in most cases they provide a good estimate of the relative AHP amplitude as function of time from the previous spike (cf. Figure 8A in Powers & Binder 2000)."

5. ARMA model, page 7: This point is related to item 1. It is not at all clear how the ARMA model given on Page 7, as appeared to be claimed by the authors, would produce or not produce a spike output at time Y_n, given the previous history of the spike train, the kernel functions and noise input. What feature or features of the spike train is modeled by the ARMA model?

As discussed earlier in this response, the ARMA model relates the spike train and noisy stimulus. It does not predict the zero/one spike train process; rather, any `predictions' made from the model should be interpreted as probabilities or rates of firing. Higher model output values indicate an interval where a spike is more likely to occur. This clarification has been added to the text in the Data Analysis section following the equation for the ARMA model.

6. Page 7 A trivial matter. It appears that the word processing package used by the authors did not treat the expression for the ARMA model kindly: aside from missing out a bracket, the superscript and subscripts for the summation signs need to be put in the correct place.

We have completely rewritten the Appendix and have carefully checked the equations. The expression now reads:

$$Z_n = \sum_{j=1}^{q} a_j X_{n-j} + \sum_{j=1}^{p} b_j Z_{n-j} + R_n$$

where $Z_n = Y_n - \mu$

7. Appendix, Page 19: Either there is a misprint in the expression oft χ_j or a substantial explanation for its form is required. Are the second set of Xs meant to be Y's?

8. Appendix, Page 19: the validity of the "circular extention" needs to be justified. It is understandable why it is done from a computational perspective, but the implication of this procedure is that the input to the neuron is periodic, which is not consistent with the expression given for the noise stimulus on page 5. The periodic extension used by the authors to describe the first N values of X seems to be inconsistent with the assumption X follows form an AR1 model. The authors must explain why this procedure does not influence any of the inferences that they draw from their results.

9. Appendix, Page 19: The issue of sampling variability comes up again – see Item 4. The authors claim a "very good approximation to β. It is difficult to know what this assertion means, but in any case it needs to be substantiated. What is the sampling variability of the esitmate of β? It is necessary to know this variability if one is to claim that certain experimental procedures alter β.

We have completely reformulated the Appendix to provide a more accurate description of how we estimated the ARMA coefficients. The new version notes that asymptotically the true least squares and circularly extended least squares estimates converge to one another and to the true values.

This convergence is what we meant in the previous version of the APPENDIX when we stated the least squares estimator to be a "very good approximation to beta".

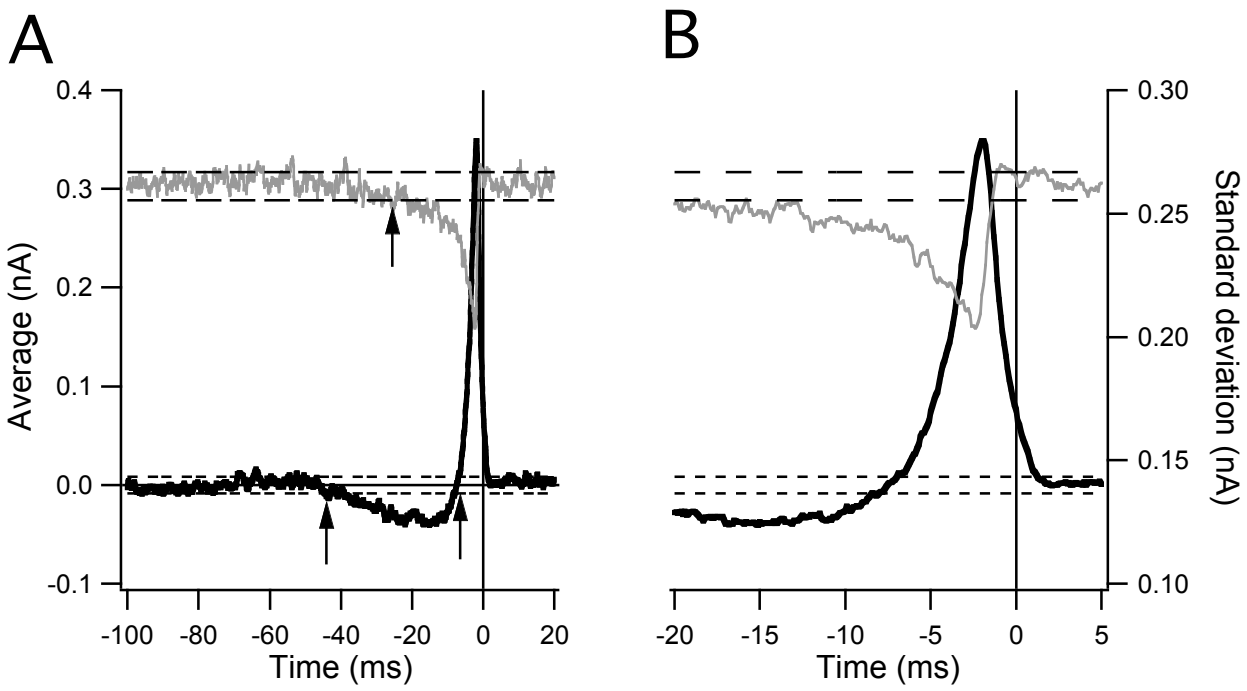
A
B
0.4
0.3
0.2
0.1
0.0
-0.1
Average (nA)
-100
-80
-60
-40
-20
0
20
Time (ms)
0.30
0.25
0.20
0.15
0.10
Standard deviation (nA)
-20
-15
-10
-5
0
5
Time (ms)

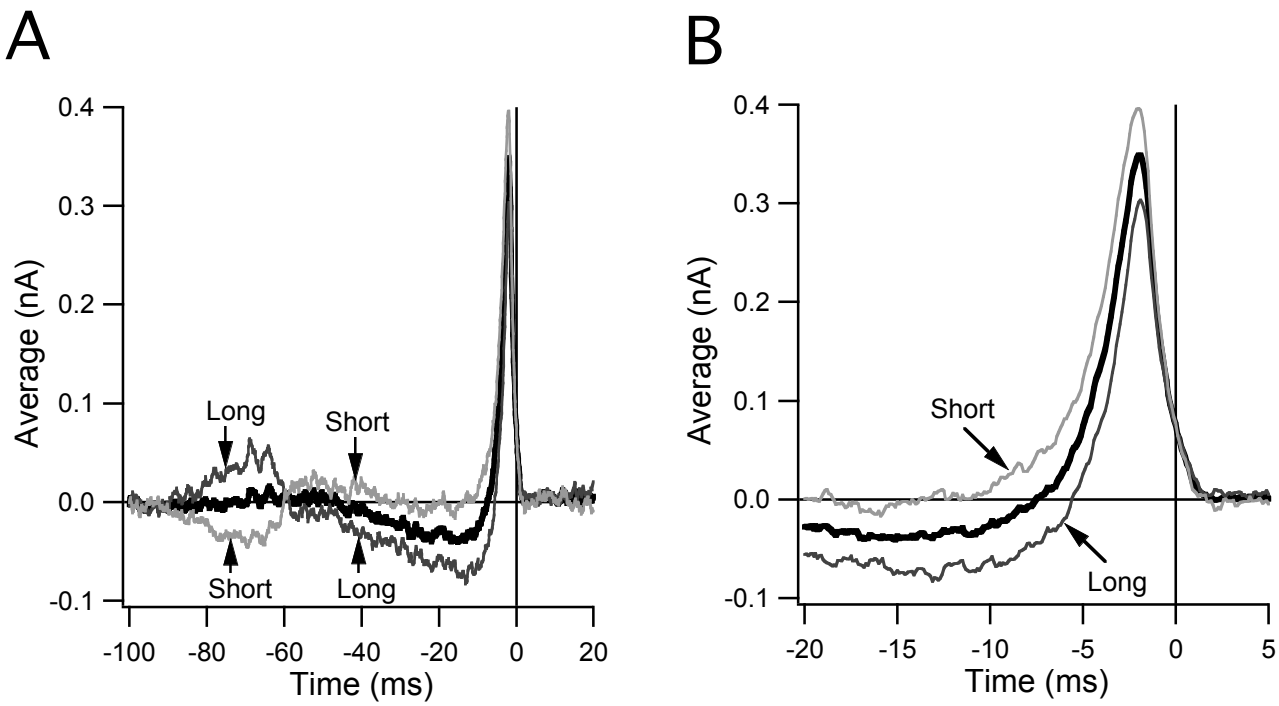
A
0.4
0.3
0.2
0.1
0.0
-0.1
Average (nA)
Long
Short
Short
Long
-100
-80
-60
-40
-20
0
20
Time (ms)
B
0.4
0.3
0.2
0.1
0.0
-0.1
Average (nA)
Short
Long
-20
-15
-10
-5
0
5
Time (ms)

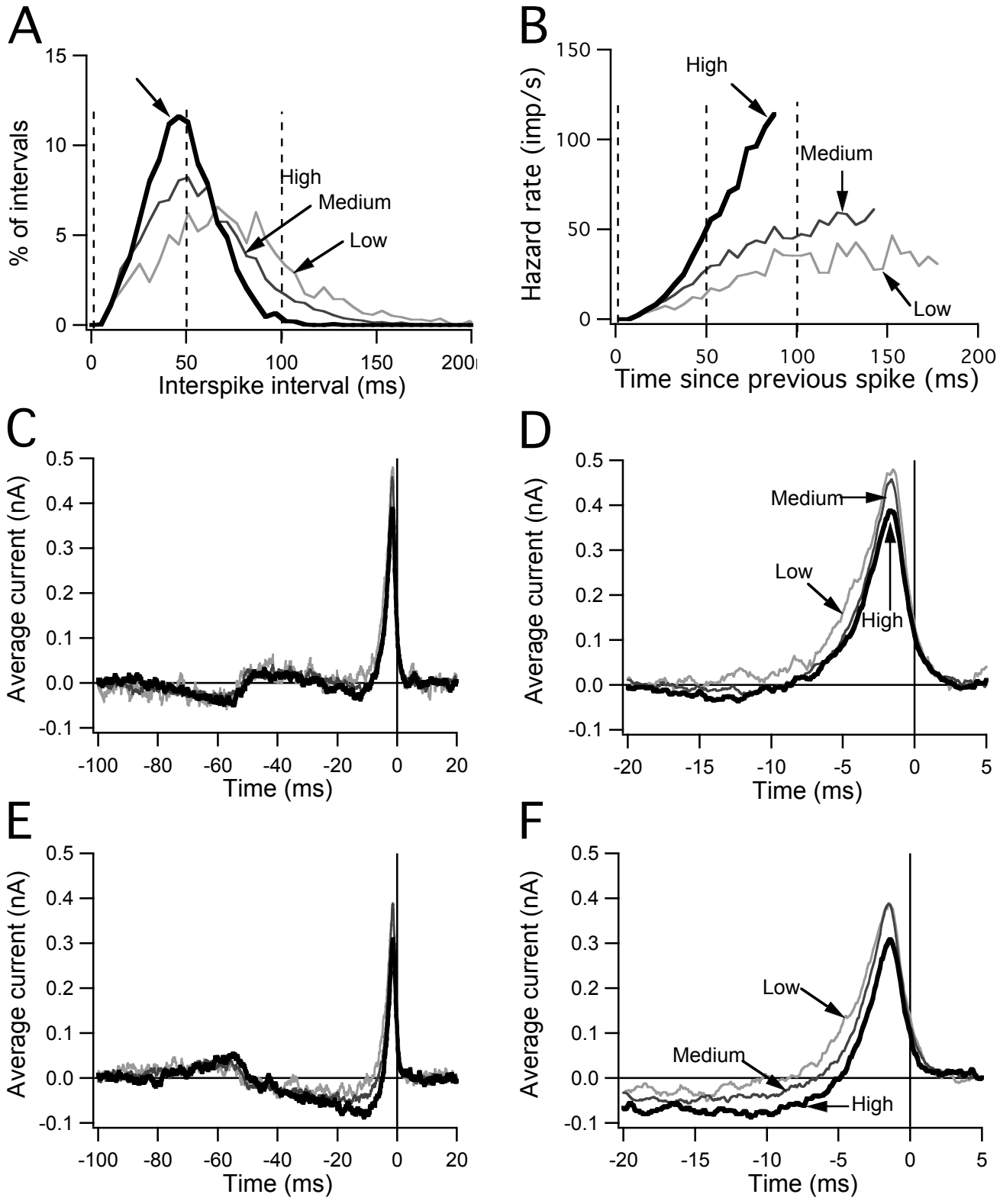
A
% of intervals
Interspike interval (ms)
High
Medium
Low
B
Hazard rate (imp/s)
Time since previous spike (ms)
High
Medium
Low
C
Average current (nA)
Time (ms)
D
Average current (nA)
Time (ms)
Medium
Low
High
E
Average current (nA)
Time (ms)
F
Average current (nA)
Time (ms)
Low
Medium
High

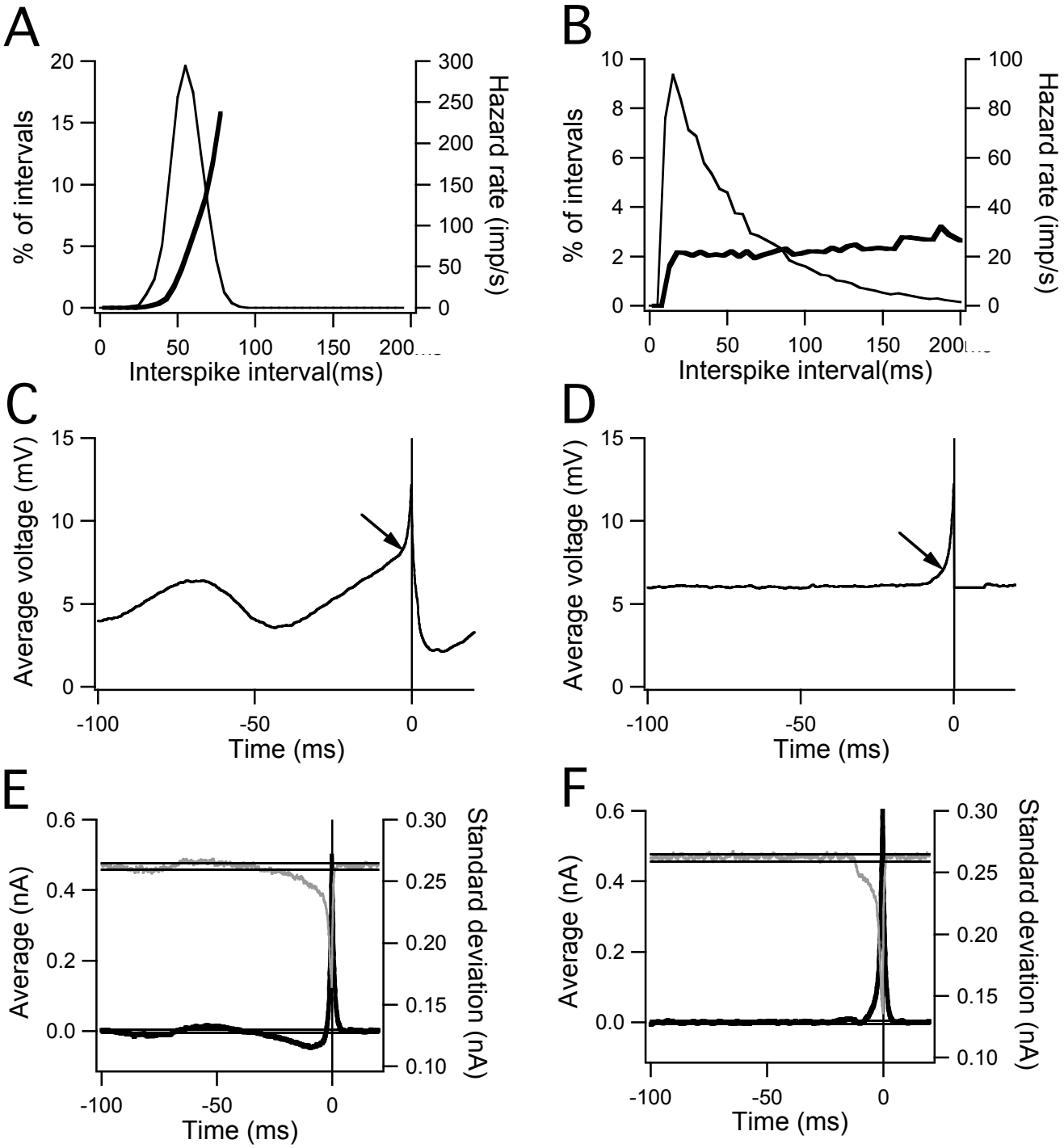
A
% of intervals
Hazard rate (imp/s)
Interspike interval(ms)
B
% of intervals
Hazard rate (imp/s)
Interspike interval(ms)
C
Average voltage (mV)
Time (ms)
D
Average voltage (mV)
Time (ms)
E
Average (nA)
Standard deviation (nA)
Time (ms)
F
Average (nA)
Standard deviation (nA)
Time (ms)

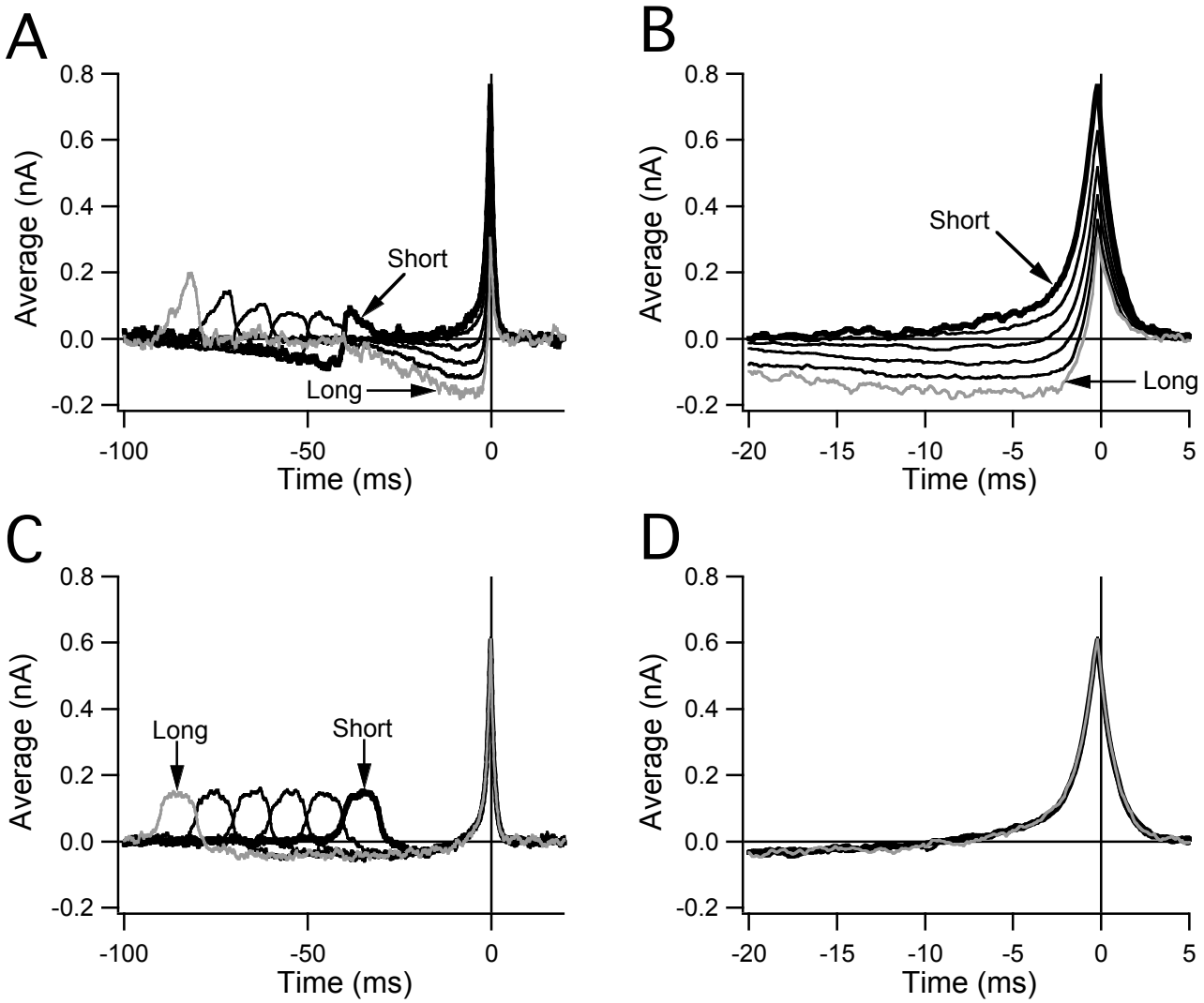
A
B
C
D
Average (nA)
Time (ms)
Short
Long
0.8
0.6
0.4
0.2
0.0
-0.2
-100
-50
0
-20
-15
-10
-5
5

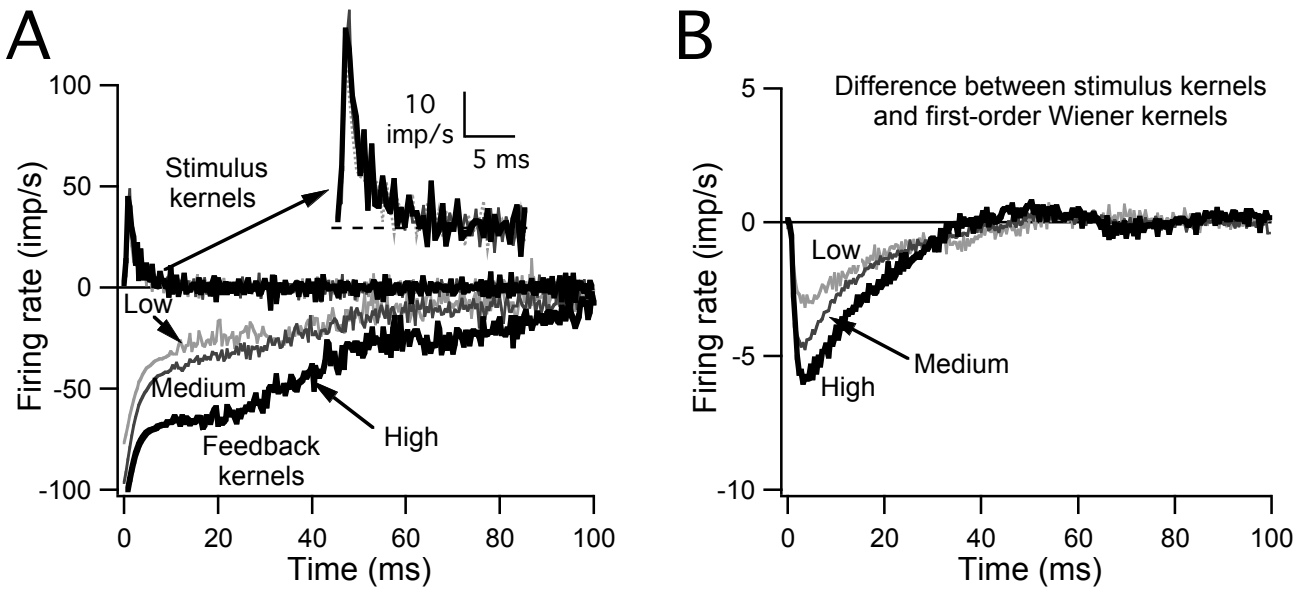
A
100
50
0
-50
-100
Firing rate (imp/s)
10
imp/s
5 ms
Stimulus
kernels
Low
Medium
High
Feedback
kernels
0
20
40
60
80
100
Time (ms)
B
Difference between stimulus kernels
and first-order Wiener kernels
5
0
-5
-10
Firing rate (imp/s)
Low
Medium
High
0
20
40
60
80
100
Time (ms)

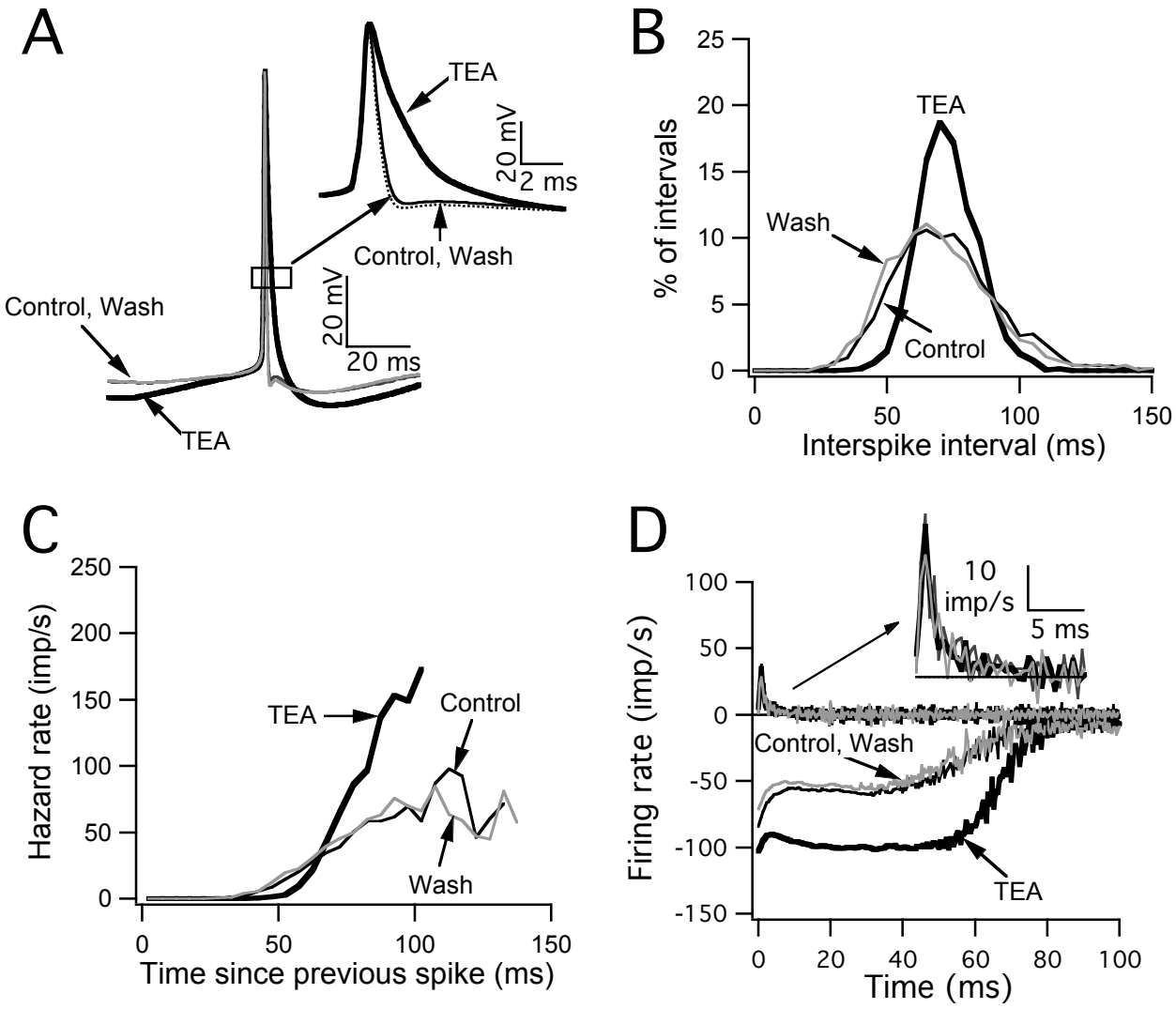
A
TEA
20 mV
2 ms
Control, Wash
Control, Wash
20 mV
20 ms
TEA
B
% of intervals
TEA
Wash
Control
Interspike interval (ms)
C
Hazard rate (imp/s)
TEA
Control
Wash
Time since previous spike (ms)
D
Firing rate (imp/s)
10
imp/s
5 ms
Control, Wash
TEA
Time (ms)

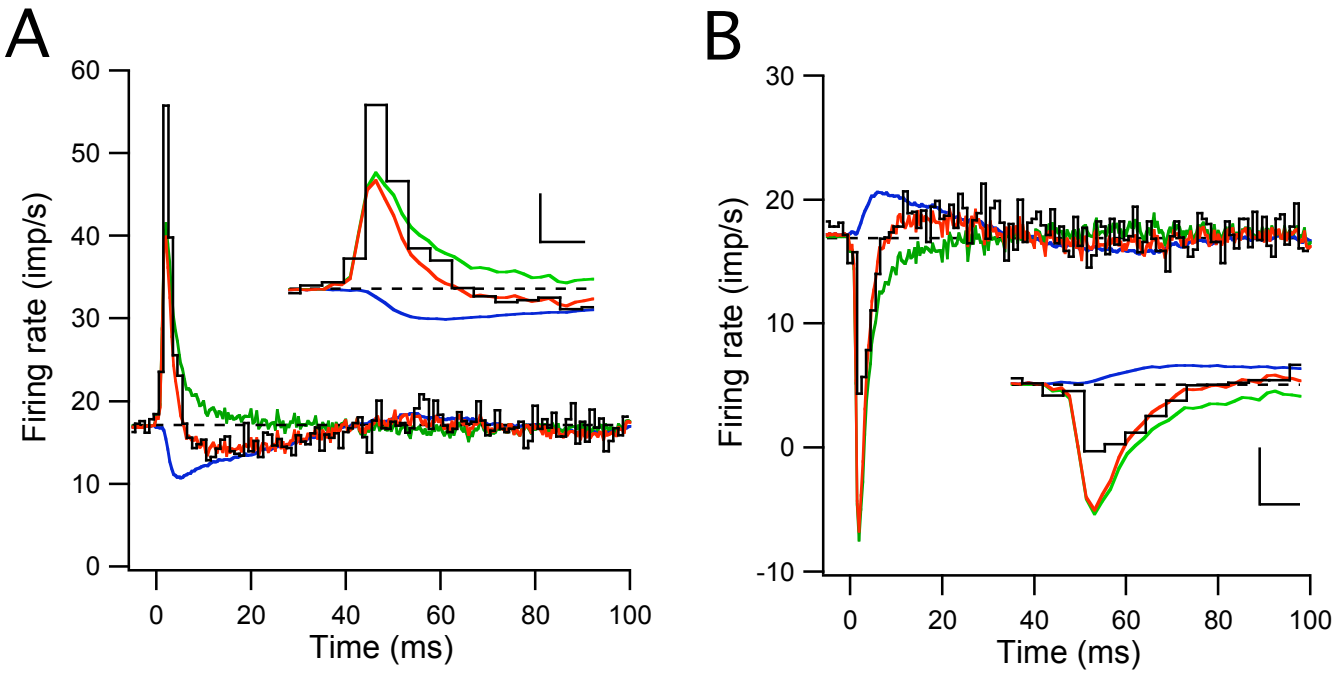
A
B
Firing rate (imp/s)
Time (ms)
0
10
20
30
40
50
60
-10
0
20
40
60
80
100